Multiple scattering description of multicenter coherent emission with applications to photoionization and electron scattering in diatomic molecules

Nodoka Hara [,1] Keisuke Hatada [,1] and Calogero R. Natoli [2,*]

[1]*Department of Physics, University of Toyama, Gofuku 3190, Toyama 930-8555, Japan*
[2]*INFN Laboratori Nazionali di Frascati, c.p. 13, I-00044 Frascati, Italy*

In the light of a multiple scattering (MS) description of molecular photodiffraction and photoabsorption processes, we present an investigation of the interplay between initial state coherence and intramolecular scattering, leading to a reinterpretation of the molecular interference in diatomic molecules and in particular of the Cohen-Fano (CF) interference term in photoabsorption. Indeed, the delocalization of the initial state electron over different atoms at positions $\mathbf{R}_n$ introduces in the language of MS theory as many virtual emitters as there are atoms in the molecule, giving rise to new MS paths as compared to the case of a single emitter. Their emission amplitudes interfere via the usual phase factor $e^{i\mathbf{k}\cdot\mathbf{R}_n}$ and in the case of two emitter photoemission describe how the usual picture of the microscopic Young's experiment is modified by the presence of intramolecular scattering. Photoabsorption follows from photoemission by integrating over the emission directions of the photoelectron and characterizes the CF oscillations as the remnants on the energy scale of the photoemission interference patterns introduced by the new paths joining the two centers, exactly like the extended x-ray absorption fine structure signals are the remnants of the closed paths that begin and end at the same atom. In the same context of initial state coherence we also show that the orientationally averaged scattering of electrons off small molecules can give access to CF type of oscillations, although in a more complicated way, due to the lack of site selectivity in comparison with the photoemission process and the absence of a dipole selection rule. It is shown that this type of modulation has the same physical origin as that found in photoabsorption.

I. INTRODUCTION

Since the seminal paper by Cohen and Fano (CF) [1] in 1966 describing the interference effect of the delocalization of the initial $1\sigma_{g,u}$ core state in the K-edge photoabsorption of the N_2 molecule, 35 years elapsed to find the experimental evidence of the predicted effect in H_2 [2] and almost 40 years for N_2 [3,4]. The effect was regarded as the manifestation of a kind of molecular double slit experiment, because photoelectrons can be emitted coherently from the two equivalent atoms in these molecules. In particular, the work of the authors in Ref. [2] about coherent emission from H_2 molecules by impact of energetic charged ion, has inspired an intense research activity on the subject that is still going on. We refer the interested reader to the paper of Ciappina *et al.* [5] for a comprehensive review on the theoretical interpretation of these phenomena. In this work we want to limit ourself to the interpretation of photoionization experiments with a minor digression to electron scattering processes.

In Ref. [3] the author shows that inversion symmetry indeed causes nonlocal, coherent behavior of the core electron photoemission from homonuclear diatomic molecules such as N_2 and that this nonlocality changes in a continuous way into a partially localized behavior, if inversion symmetry is violated by isotopic nuclear substitution.

Shortly after Zimmermann *et al.* [6] investigated the relation between intramolecular scattering and CF interference

in photoelectron diffraction experiments on the isoelectronic hetero- and homonuclear molecules, CO and N_2, in the gas phase, reaching the conclusion that there are two kinds of processes: A two-center interference between two spatially coherent emitters in the case of N_2 and one-center self-interference in the case of CO, the latter being the signature of a loss of spatial coherence.

The idea behind this interpretation is that the indistinguishability of the emission pathways caused by the inversion symmetry of the N_2 molecule leads to coherent emission of photoelectron waves from both molecular centers, whereas this process is not possible in the CO molecule due to the distinguishability of the emission sites.

For a certain period the symmetry equivalence of the emitters was considered essential for the observation of the CF interference effect, so that it came to a surprise [7] when Canton *et al.* found evidence of the effect in the vibrationally resolved photoionization of the $1\pi^{-1}$ valence state of the heteropolar molecule CO [8].

In view of these findings it would be very useful to have a conceptual framework in which to describe all these phenomena. The purpose of this paper is to present such a unifying theoretical framework based on multiple scattering (MS) theory, in the light of the concept of atomic coherence of the initial state (as specified below) that does not necessarily require the equivalence of the emitters to cause interference. The ensuing analysis will lead to a different interpretation of the physical meaning of the interference phenomena than hitherto attributed to them.

*natoli@lnf.infn.it

It is by now well established that MS theory is the language of election for the description of many types of spectroscopy, including photoabsorption and photoelectron diffraction [9–11]. Based on the Full Potential formulation of MS theory [12], one has now the possibility of generating exact numerical solutions of the Schrödinger equation (SE) for bound or continuum states, which are the ingredients for the description of many spectroscopies in the independent quasiparticle approach. Indeed, a great advantage of MS theory is that one can write the response function of the various spectroscopies only in terms of the scattering path operator τ, which provides at the same time an intuitive physical description of the processes under consideration. For example, it highlights the coherence of the various atomic emission processes (even virtual) and their connection with the atomic structure. In this respect the use of MS theory for describing these virtual emissions in relation to interference processes is nearly irreplaceable for the insight it provides into the working of quantum mechanics.

In the following we shall use the length form of the dipole operator. Disregarding the presence of the core and valence hole, in our independent particle picture approach both initial and final states are eigenstates of the same Hamiltonian and therefore the length and velocity gauge should give identical results. Even in this ideal situation, the numerical approximations (the angular momentum expansion around each center is truncated to an l_{max} value, neglect of the contribution of the outer sphere region to the integral of the transition matrix element...) make the two gauges slightly different, up to a 10–15% in some cases, though in general they present the same shape. (A comparison between calculated cross sections in the two gauges is given in Fig. 7.)

Taking into account the presence of the core and valence hole (by considering some kind of static charge self-consistent relaxation around the hole in the final state) introduces further uncertainties. Indeed, a satisfactory treatment of the dynamical effects of the hole in the final is still an unsolved problem. Therefore, even in the assumption that the various gauges gave the same answer, we would be still confronted with an approximate description of the effect of the hole. The important point, however, is that the transition matrix elements of the cell around each atom [$M_L^n(E)$ in Eq. (13)] are featureless both for core and valence states. The amplitudes $B_L^n(\mathbf{k})$ in Eq. (14), which describe the physics of the process, are only slightly affected by this uncertainty. This aspect of MS theory has been exploited in the past in relation to structural analysis [11,13].

There is no problem in accounting for the presence of the core hole in the final state, if the initial core state is localized on one atom. One promotes the core electron to the first available non occupied state of the system under consideration (crystal, cluster of atom, etc.) to mimic some sort of static screening of the core hole, using the self-consistent charge density of this configuration to calculate the final state core-hole potential [14]. Note however that the calculations with and without core hole do not differ significantly in relations to the questions discussed in this paper.

When the initial core state is delocalized on two equivalent atoms (valence-like core state), such as the $1\sigma_{g,u}$ states in N_2, our *ansatz* is to use a self-consistent charge density with a hole in the same delocalized initial state and an electron promoted

to the first available non occupied state of the same symmetry. The resulting core hole potential has therefore the same symmetry as the initial state. This approach is inspired by the nonorthogonal configuration interaction (NOCI) method used to describe the molecule with a core hole by making proper, symmetry adapted, linear combinations of the degenerate localized solutions, in which the core hole is localized in turn on the various equivalent atoms [15].

Throughout this paper we shall use atomic units (a.u.) for lengths and Rydberg units for energies, unless otherwise stated. Moreover, we have followed the literature in material science, whereby photoemission implies the detection of photoelectron outside the system, whereas in photoabsorption one measures the attenuation of the photon beam after passing trough the sample.

In the organization of the paper we distinguish between the two spectroscopies. Even though both of them are expression of the same physical process (photoionization) and are described in terms of coherent emission from atomic centers, the experimental apparatus is different in the two cases. As discussed below in photoemission one measures the diffraction patterns of the emitted electrons, whereas in absorption one measures the number of holes created by the incoming photons. Therefore, one cannot expect the same interference patterns in the two spectroscopies nor the same physical meaning. Sections II and III and relative subsections deal with photoemission, while Sec. IV and its subsections deal with photoabsorption. In particular Sec. II presents the way to write the photoemission cross section in the language of multiple scattering theory (MST) both for the initial and the final states, this latter expressed in terms of the scattering amplitudes $B_L^n(\mathbf{k})$ centered at each molecular site n. Section II A describes the photoemission process starting from a localized core state and gives the physical interpretation of these scattering amplitudes according to the Feynman's rules. They obey a kind of generalized optical theorem given in Eq. (10) which is essential to establish the relation between photoemission and photoabsorption cross section. Section III gives the general expression to calculate the cross section of photoemission from valence states, where Eq. (12) presents the process as a coherent sum of virtual core-like excitations, each emanating from one of the various molecular sites, weighted by the phase factor $e^{i\mathbf{k}\cdot\mathbf{R}_n}$. Section III A specializes this formula to the case of heteropolar diatomic molecules, whereas Sec. III B deals with the case of photoemission in homopolar diatomic molecules and illustrate how the usual picture of the microscopic Young's experiment is modified by the presence of intramolecular scattering. Section III C calculates the photoelectron diffraction along the molecular axis in N_2 and CO using an exact expression calculated in the Appendix A 2, to interpret the experimental findings of Ref. [6] and elucidates the relation between intramolecular scattering and CF interference. Section IV uses Eq. (12) of Sec. III and the generalized optical theorem for the photoemission scattering amplitudes to derive the exact photoabsorption cross section in the framework of our independent particle approach, both for heteropolar and homopolar diatomic molecules. The case of CO absorption is treated to illustrate the role of photon polarization in determining the presence or absence of MS oscillations in the spectrum. Section IV A derives the Cohen-

Fano interference term in the framework of the present theory using the Born Approximation for the scattering path operator $\boldsymbol{\tau}$, for photon polarization along and perpendicular to the molecular axis, and compares with the original derivation by Cohen and Fano [1]. It is shown that both the extended x-ray absorption fine structure (EXAFS) and CF oscillations have the same physical origin, being the remnants on the energy scale of the corresponding photodiffraction patterns, after averaging over the emission angles. Section IV B studies the conditions of validity of the Born approximation with application to the oscillatory structure of N_2 valence photoabsorption ionization cross section. The corresponding signal is compared with the experimental data by Ilchen *et al.* [16], deriving in this way the correct molecular bond length. Section IV C presents an analysis of the photoabsorption cross section in the whole spectral range, based on Eq. (25). It gives an explanation of why the shape resonance is missing in the case of the ungerade initial state. Section IV D discusses the question of the Cooper-like minima in the partial absorption cross sections and their relation with the CF modulations in the total cross section, showing clearly that they are not related to some kind of intra molecular confinement of the excited photoelectron, as suggested by some authors [17]. Section IV E illustrates the CF formula in the case of photoabsorption in heteropolar diatomic molecules, showing that this kind of signal can also be observed in molecules like CO, depending on the values of the mixing coefficients c_i present in the initial valence state. Finally, Sec. V presents, in the context of initial state coherence, the derivation of the cross section for orientationally averaged scattering of electrons off diatomic molecules, that also shows the typical CF oscillations. It is shown that this type of modulation has the same physical origin as that found in photoabsorption. After this, Sec. VI draws the conclusions. Appendix A 1 summarizes, for the benefit of the reader, some of the aspects of MS theory, useful for understanding its structure, in particular the ordering of the MS paths. Appendix A 2 derives in the framework of MST the exact expression for calculating the photoelectron diffraction along the molecular axis in N_2 and CO and Appendix A 3, using the same formalism, derives the total integrated molecular cross section in terms of the integrated partial ionization cross sections to get more insight into the mechanism of electron confinement.

II. THE PHOTOEMISSION CROSS SECTION IN THE FRAMEWORK OF MULTIPLE SCATTERING THEORY

In the independent particle approach the initial and final states of the system are Slater determinants (SD) so that, taking into account the presence of the core hole in the final state by a static potential when needed, the photoemission cross section for the ejection of a photoelectron along the direction $\hat{\mathbf{k}}$ is given by

$$\frac{d\sigma}{d\hat{\mathbf{k}}} = 4\pi^2 \alpha \hbar \omega \left| \int d\mathbf{r} \, [\psi_{\mathbf{k}}^{-}(\mathbf{r})]^* \, (e^{i\kappa \cdot \mathbf{r}} \, \mathbf{e} \cdot \mathbf{r}) \, \Phi_{c,v}(\mathbf{r}) \right|^2, \quad (1)$$

where $\alpha = 1/137$ is the fine structure constant, $\hbar \omega$ is the incoming photon energy with real polarization vector $\mathbf{e}$, $\Phi_{c,v}(\mathbf{r})$ is the initial core (valence) wave function and $\psi_{\mathbf{k}}^{-}(\mathbf{r})$ is the time reversal of the continuum scattering state $\psi_{\mathbf{k}}^{+}(\mathbf{r})$ describ-

ing the excited photoelectron. The time reversal is necessary to impose the boundary condition that no electron exists in a continuum state in the remote past. Neglecting spin degrees of freedom, $\psi_{\mathbf{k}}^{-}(\mathbf{r}) = [\psi_{\mathbf{k}}^{+}(\mathbf{r})]^*$. In Eq. (1) we have kept the exponential factor originating from the vector potential of the impinging photon with wave vector κ, neglecting terms proportional to $\kappa \cdot \mathbf{p}$ and κ^2, where $\mathbf{p}$ is the electron momentum. It should be kept in mind if one intends to highlight the self-interference of the incoming photon in the coherent photoionization, but in the following applications it can be and was actually set equal to one with a good approximation.

The continuum state $|\psi_{\mathbf{k}}^{+}(\mathbf{r})\rangle$ satisfies the SE with positive energy ($k = \sqrt{E}$)

$$[\nabla^2 + E - V_{\text{eff}}(\mathbf{r})] \, \psi_{\mathbf{k}}^{+}(\mathbf{r}) = 0, \quad (2)$$

with outgoing wave boundary condition and normalization to one state per Rydberg

$$\psi_{\mathbf{k}}^{+}(\mathbf{r}) \asymp \left(\frac{k}{16\pi^3} \right)^{\frac{1}{2}} \left[e^{i\mathbf{k} \cdot \mathbf{r}} + f(\hat{\mathbf{r}}; \mathbf{k}) \frac{e^{ikr}}{r} \right]. \quad (3)$$

In Eq. (2) $V_{\text{eff}}(\mathbf{r})$ represents an effective optical potential, in general complex, coming from the reduction of the many-body problem to an effective one-particle problem. Without loss of generality for the present discussion, we assume that $V_{\text{eff}}(\mathbf{r})$ is a real potential. We shall use throughout the real Hedin-Lundqvist potential (HL) [18]. The role of the complex part of the potential is to dampen the effects of the coherent interference. Details of the reduction process and of the role of a complex potential are provided in Ref. [9].

As is well known, multiple scattering theory is a technique for solving a linear partial differential equation over a region of space with certain boundary conditions. It is implemented by dividing the space into nonoverlapping domains Ω_i (cells), solving the differential equation separately in each of the cells and then assembling together the partial solutions into a global solution that is continuous and smooth across the whole region and satisfies the given boundary conditions.

As a consequence, both the initial and final state, global solutions of the SE, can be represented in each cell by a linear combination of suitably normalized local solutions times coefficients depending on the imposed boundary conditions.

For initial valence states, without loss of generality, in each cell Ω_i we can write the global solution as

$$\Phi_{c,v}(\mathbf{r}_i) = \sum_L C_L^i \, \phi_L^v(\mathbf{r}_i), \quad (4)$$

where $\mathbf{r}_i = \mathbf{r} - \mathbf{R}_i$ is the local coordinate referred to the center of the cell $\mathbf{R}_i$ and $\phi_L^v(\mathbf{r}_i)$ are regular local solutions of the SE for bound states behaving at the origin like $r^l Y_L(\hat{\mathbf{r}})$. As usual, L stands for the pair l, m of angular momentum indices and $Y_L(\hat{\mathbf{r}})$ is a real Spherical Harmonics. Global normalization requires that

$$\sum_{iL} \left| C_L^i \right|^2 \int_{\Omega_i} d\mathbf{r}_i \left| \phi_L^v(\mathbf{r}_i) \right|^2 = 1, \quad (5)$$

assuming that the various $\phi_L^v(\mathbf{r}_i)$ are orthogonal in the L basis. An initial state with support in different cells is said to have atomic coherence.

A core state completely localized in the cell Ω_c, with a definite angular momentum L_c, is obtained by taking all the coefficients $C_L^i = 0$, except for $i = c$ and $L = L_c$. In this case $C_{L_c}^c = 1$, since the core wave function $\phi_{L_c}^c(\mathbf{r}_i)$ is normalized to one in the cell.

Similarly, the excited continuum state $\psi_{\mathbf{k}}^+(\mathbf{r})$ can be represented locally by the expression

$$\psi_{\mathbf{k}}^+(\mathbf{r}_i) = \sum_L B_L^i(\mathbf{k})\,\Phi_L^i(\mathbf{r}_i; k), \qquad (6)$$

where the index $\mathbf{k}$ is reminiscent of the boundary conditions Eq. (3) and $\Phi_L^i(\mathbf{r}_i; k)$ is a suitably normalized local solution of the SE in cell Ω_i [12]. The coefficients $B_L^i(\mathbf{k})$, together with their physical meaning, will be discussed extensively in the next section.

A. Photoemission from a localized core state

In this case, we assume that the initial core state is localized inside the cell Ω_c at site c. Then the matrix element in Eq. (1) becomes

$$\frac{d\sigma}{d\hat{\mathbf{k}}} = 4\pi^2\alpha\,\hbar\omega \sum_{m_c} \left| \sum_L M_{L_c\,L}^{\mathbf{e}}(E)\,[B_L^c(\mathbf{k})]^{\star} \right|^2. \qquad (7)$$

Here we have introduced the atomic transition matrix element

$$M_{L_c\,L}^{\mathbf{e}}(E) = \int_{\Omega_c} d\,\mathbf{r}_c\,\left(\Phi_L^c(\mathbf{r}_c; k)\right)^{\star}(\mathbf{e}\cdot\mathbf{r}_c)\,\phi_{L_c}^c(\mathbf{r}_c), \qquad (8)$$

where the superscript $\mathbf{e}$ indicates the dependence on the incoming photon polarization. The role of this latter is to determine the escape direction of the photoelectron according to the final angular momentum L selected by the dipole selection rule with amplitude $Y_L(\hat{\mathbf{r}})$. For typographical convenience it will be omitted in the following.

By performing the sum over the linear components $\mathbf{e}_m$ before the square modulus one obtains the unpolarized cross section.

In Appendix A 1 we show that the scattering amplitude $B_L^c(\mathbf{k})$ is given by

$$B_L^c(\mathbf{k}) = \sqrt{\frac{k}{\pi}}\,\sum_{jL'} \tau_{LL'}^{c\,j}\,i^{l'}\,Y_{L'}(\hat{\mathbf{k}})\,e^{i\mathbf{k}\cdot\mathbf{R}_j}, \qquad (9)$$

where $\tau_{LL'}^{i\,j}$ represents the full scattering path operator, giving the total amplitude of propagation of the photoelectron from site i to site j, starting with angular momentum L around site i and arriving with angular momentum L' at site j.

Due to the expression (9) we obtain the photoelectron diffraction (PED) cross section by taking the product of the amplitude $M_{L_c\,L}$ for creating a photoelectron in a state of spherical wave L selected by the dipole selection rule from an initial core state L_c, times the amplitude of propagation from site c to any site j, starting with angular momentum L and ending with angular momentum L' after any number of scattering events, times the phase difference $e^{i\mathbf{k}\cdot\mathbf{R}_j}$ of the photoelectronic wave between the initial and final sites c and j, times the spherical wave amplitude $i^{l'}Y_{L'}(\hat{\mathbf{k}})$ for escaping toward the detector. All these amplitudes are to be summed together and squared to obtain the intensity of the photoelectron current at the detector, in keeping with the Feynman's rules

for composite consecutive events [19] and alternative paths to the same final state.

It is clear that the interference patterns so measured by the detector depend on the actual positions of the atoms in the sample and represent a three-dimensional hologram of the sample-object (i.e., the atomic positions in the system under study) in momentum and energy space, associated with the three degrees of freedom of the two polar and azimuthal emission angles and the final kinetic energy of the photoelectron, as pointed out by Ref. [20]. For an in depth discussion on this aspect also from an experimental point of view see Ref. [21].

In case of real potentials the scattering amplitudes $B_L^i(\mathbf{k})$ satisfy the relation

$$\int d\hat{\mathbf{k}}\,B_L^i(\mathbf{k})\,\left[B_{L'}^j(\mathbf{k})\right]^* = -\frac{1}{\pi}\,\Im\,\tau_{LL'}^{i\,j}, \qquad (10)$$

which is a kind of generalized optical theorem, consequence of the conservation of particle flux. This relation is very important, since it establishes the connection between the photoemission and the photoabsorption cross sections [12].

In fact, by integrating the PED cross section over all emission angles and exploiting Eq. (10) we get

$$\int d\hat{\mathbf{k}}\,\frac{d\sigma}{d\hat{\mathbf{k}}} = 4\pi^2\alpha\,\hbar\,\omega \sum_{m_c}\int d\hat{\mathbf{k}} \left| \sum_L M_{L_c L}(E)\,[B_L^c(\mathbf{k})]^* \right|^2$$

$$= -4\pi\,\alpha\,\hbar\,\omega \sum_{LL'm_c} M_{L_c L}(E)\,\Im\tau_{LL'}^{c\,c}M_{L_c L'}^{\star}, \qquad (11)$$

which is equal to the absorption cross section [9].

As a consequence, the integration process eliminates the physical detector located outside the sample and replaces it by the atomic emitter (since we count the number of holes), which becomes in this way both the source and the detector of the photoelectrons.

According to Feynman's rules we can interpret the second line of Eq. (11) as the imaginary part of the amplitude for creating an electron at the site of the photoabsorber, times the amplitude of propagation from this site to the same site after undergoing any number of multiple scattering by the atoms in the system, times the amplitude of being re-absorbed at the emitter atom. A typical such contribution to the absorption cross section are the oscillations of period $\Delta k = \pi/R$, that are due to the interference between the outgoing photoelectronic wave from the emitter and the returning wave after a single back-scattering from a neighbor at distance R. They are known as EXAFS oscillations.

III. PHOTOEMISSION FROM MOLECULAR VALENCE STATES

Remembering Eq. (4), photoemission from molecular valence states can be written as

$$\frac{d\sigma}{d\hat{\mathbf{k}}} = 4\pi^2\alpha\,\hbar\omega \left| \sum_n \sum_L M_L^n(E)\,[B_L^n(\mathbf{k})]^{\star} \right|^2$$

$$= 4\pi^2\alpha\,\hbar\omega \left| \sum_n e^{-i\mathbf{k}\cdot\mathbf{R}_n} \sum_L M_L^n(E)\,[\overline{B}_L^n(\mathbf{k})]^{\star} \right|^2, \qquad (12)$$
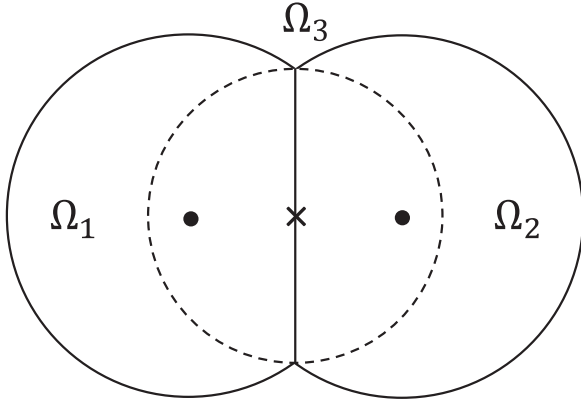
FIG. 1. Minimal space partitioning for a diatomic molecule.

where we have partitioned the molecular volume in cells Ω_n so that

$$M_L^n (E) = \sum_\Lambda C_\Lambda^n \int_{\Omega_n} d\,\mathbf{r}_n \big[\Phi_L^n(\mathbf{r}_n; k) \big]^\star (\mathbf{e} \cdot \mathbf{r}_n)\, \phi_\Lambda^v(\mathbf{r}_n).$$

(13)

In the second equation (12) we have introduced the quantity

$$\overline{B}_L^n(\mathbf{k}) = \sqrt{\frac{k}{\pi}} \sum_{jL'} \tau_{LL'}^{n\,j}\, i^{l'}\, Y_{L'}(\hat{\mathbf{k}})\, e^{i\mathbf{k}\cdot(\mathbf{R}_j - \mathbf{R}_n)},$$

(14)

which in a periodic system is translationally invariant. Remembering Eq. (1), we have omitted in Eqs. (12) and (13) a phase factor $e^{i\boldsymbol{\kappa}\cdot\mathbf{R}_n}$ which would arise from the fact that the vector potential of the photon is referred to the common origin of the atomic coordinates $\mathbf{R}_n$, representing the self-interference of the incoming photon. It can be neglected with respect to the photoelectron wave vector for energies up to 1000 eV for shallow initial states.

Equation (12) is particularly suggestive, in that it describes the photoemission from a valence initial state as a coherent sum of core-like photoemission amplitudes, each processes emanating from one of the various molecular sites, weighted by the phase factor $e^{-i\mathbf{k}\cdot\mathbf{R}_n}$.

Emission from valence molecular states in terms of photoelectron wave interference, caused by initial state delocalization and final state photoelectron scattering has also been treated by Krüger in Ref. [22], but without making explicit reference to the structural phase factor.

In the following we shall specialize the above equations to diatomic molecules in the framework of full potential multiple scattering (FPMS) theory [12]. Figure 1 shows a minimal partition of the space into two cells Ω_1 and Ω_2 around the physical atoms and a third region Ω_3 comprising the rest of the space. For all considered valence states of the diatomic molecules mentioned below, we found that the contribution to the photoemission and photoabsorption cross section of region Ω_3 can be neglected, due to its small contribution to the normalization integral and therefore to the transition matrix elements involved in the expression of the cross section. Indeed, calculations carried out using the above minimal partition, and one in which region Ω_3 is replaced by a sufficient number of empty cells covering the space until the

external molecular potential becomes negligible, do not show meaningful differences. We are therefore confident that we can describe the physical properties of the diatomic molecules by considering only the regions Ω_1 and Ω_2. In the following all our calculations are carried out in full potential mode, including therefore the anisotropies of the molecular potential, and by inverting exactly the MS matrix $(\mathbf{T}^{-1} - \mathbf{G}) = \boldsymbol{\tau}^{-1}$, except when explicitly stated otherwise.

A. Photoemission in heteropolar diatomic molecules

In the case of diatomic molecules we assume that the two atoms are located along the z axis at $\mathbf{R}_1 = (0, 0, -R/2)$ and $\mathbf{R}_2 = (0, 0, R/2)$, R being the interatomic bond length. For future reference, we shall take $R = 1.1$ Å for N_2 and $R = 1.13$ Å for CO.

In the framework of MST we can write the initial valence state in the heteropolar case as

$$\phi_{is}^v(\mathbf{r}) = c_1\, \phi_1(\mathbf{r}_1) + c_2\, \phi_2(\mathbf{r}_2) + c_3\, \phi_3(\mathbf{r}_3),$$

(15)

where each function $\phi_i(\mathbf{r}_i)$ has support only in the cell Ω_i. The normalization condition imposes that

$$\sum_{i=1,3} c_i^2 \int_{\Omega_i} d\mathbf{r}_i\, |\phi_i(\mathbf{r}_i)|^2 = 1.$$

(16)

As anticipated above, we neglect the wave function in region Ω_3 and renormalize the two coefficients c_i ($i = 1, 2$) accordingly. Then the photoemission cross section can be written as

$$\frac{d\sigma}{d\hat{\mathbf{k}}} = 4\pi^2 \alpha\, \hbar\omega \left| \sum_L \big(c_1 [M_L^1(E)]^* \overline{B}_L^1(\mathbf{k}) \right.$$
$$\left. + c_2 [M_L^2(E)]^* \overline{B}_L^2(\mathbf{k}) e^{i\mathbf{k}\cdot\mathbf{R}} \big) \right|^2,$$

(17)

taking for convenience the complex conjugate of the photoemission amplitude in Eq. (12) and putting $\mathbf{R} = \mathbf{R}_2 - \mathbf{R}_1$.

This equation illustrates the role of the initial coherent delocalization of the excited photoelectron in creating interference patterns between different emitter sites. It can be used to describe the $1\pi^{-1}$ ionization of the heteropolar molecule CO. In this case the $\phi_i(\mathbf{r}_i)$ wave functions are approximately $2p$ carbon and oxygen atomic orbitals so that the main transition is to a $l = 2$ final state [8]. In the limit $c_2 \to 0$ one recovers the photoemission from a core state localized at $\mathbf{R}_1$ (and viceversa).

The case of the heteropolar molecule CO is particularly interesting, since photoemission from the K-edge of either carbon or oxygen has been considered as a double-slit experiment with only one of the two slits open, due to the inequivalence of the two atomic sites [6]. However, Eq. (17) shows that to get interference between two atomic sites it is only necessary that the initial state be delocalized over the two sites.

By looking at the extension of the two $1s$ orbitals centered on the two atomic sites we notice that the situation is similar to that of the N_2 molecule, that has an effective hopping integral (resonance integral) of 0.05 eV (half the energy gap between the bonding $(1\sigma_g)$ and the antibonding $(1\sigma_u)$ states). So we

expect a resonance integral of the same order of magnitude between the $1s$ carbon and oxygen orbitals in CO, with the consequence that even the 1σ ground state of the CO molecule is slightly delocalized and is a mixture of the two $1s$ orbitals with appropriate coefficients. We defer this discussion until after the molecular photoabsorption has been calculated.

B. Photoemission in homopolar diatomic molecules and its relation to the Young's two-slit experiment

In the case of homopolar diatomic molecules, the two atomic sites are related by inversion symmetry. For illustration purposes, in a first approximation one might consider the molecule as a periodic system with two sites, neglecting termination errors. In this case, assuming $M_L^i(E)\overline{B}_L^i$ independent from the site i and taking $c_i^2 = 1/2$, one would obtain

$$\frac{d\sigma}{d\hat{\mathbf{k}}} = 4\pi^2\alpha\,\hbar\omega \left|\sum_L M_L^*(E)\,\overline{B}_L(\mathbf{k})\right|^2 [1 \pm \cos(\mathbf{k}\cdot\mathbf{R})],\tag{18}$$

where the $+(-)$ sign is for "gerade (ungerade)" initial states. As apparent from this expression the summation over the two states eliminates the interference term and the coherent emission from the two equivalent atoms collapses to a single site emission.

Before proceeding with the discussion on the relation with the Young's two-slit experiment it is expedient to derive from Eq. (17) the photoemission equivalent of the Cohen-Fano formula in our formalism. This expression is obtained by putting in the lowest order Born approximation $B_L(\mathbf{k}) \propto t_l\, i^l\, Y_L(\hat{\mathbf{k}})$, so that assuming a final $l = 1$ angular momentum and $c_1^2 = c_2^2 = 1/2$, one finds

$$\frac{d\sigma}{d\hat{\mathbf{k}}} = \frac{1}{2}\sigma_{\text{at}}(\hbar\omega) \left|\sum_m \mathbf{e}_m Y_{1m}(\hat{\mathbf{k}})\right|^2 |1 \pm e^{i\mathbf{k}\cdot\mathbf{R}}|^2$$

$$= \sigma_{\text{at}}(\hbar\omega)(\mathbf{e}\cdot\hat{\mathbf{k}})^2 [1 + \cos(\mathbf{k}\cdot\mathbf{R})],\tag{19}$$

where again $\mathbf{e}_m$ indicates the linear components of the photon polarization vector. Here the $\hat{\mathbf{k}}$ polar angle θ is measured from the z axis where the two atoms of the molecule lie with coordinates $(0, 0, \pm R/2)$. This result coincides (except for the atomic matrix element!) with the direct calculation of the Cohen-Fano molecular matrix element as performed by Baltenkov *et al.* [23].

We now analyze the interference patterns when the photon polarization vector is perpendicular to the molecular axis. In this case we consider a plane containing the molecular axis and perpendicular to the photon polarization, and put the detector on a plane parallel to it, at a distance $d \gg R$. The angle θ' between $\hat{\mathbf{k}}$ and $\hat{\mathbf{e}}$ is complementary to the angle θ, so that $[1 + \cos(\mathbf{k}\cdot\mathbf{R})] = \{1 + \cos[kR\sin(\theta')]\}$. Hence, the condition for extinction is given by $R\sin(\theta') = n\lambda/2$, n being any positive or negative integer odd number. This is the well known formula of the directional Young's two-slit experiment. For polarization parallel to the molecular axis the detector plane can be taken orthogonal to the polarization direction. The interference pattern are then determined by the relation $\{1 + \cos[kR\cos(\theta)]\}$ and the condition for extinction is $R\cos(\theta) = n\lambda/2$, where again n is any positive

or negative odd number. In particular at $\theta = 0$ the condition becomes $kR = n\pi$, as observed in Ref. [17] and interpreted as a condition for electron confinement. Notice that if the lateral spread of the rays in the Young's experiment is large enough (reaching $\theta' = \pi/2$ and beyond), some of the two sets of extinction directions coincide.

Both situations can be physically realized by two radiating dipole antennas with charge oscillating along the z axis, separated by a distance R along the y axis at positions $(0, \pm R/2, 0)$ and observed by detectors put in two planes orthogonal, respectively, to the x and y axis at distance much greater than R.

The common physical principle underlying the two situations is coherent emission from two sources *without interference of one source onto the other*. The "classical" directional Young's two-slit experiment realizes only one of the two arrangement, but is clear that the other too can be called in his own right a "Young experiment." We might call the antenna's setup a *generalized* Young-type experiment, in keeping with other authors that call the second set of extinction conditions "Young-type" interference conditions [24].

The distinctive features that makes photoemission interference patterns different from the Young-type patterns coming from the interference factor $[1 + \cos(\mathbf{k}\cdot\mathbf{R})]$ is that photoemission patterns *do include feedback between the two emission slits*, as apparent from Eq. (18), where the emission from a single site does depend on the direction of $\mathbf{k}$. Indeed, what is modulated is the entire photoelectron diffraction pattern of the molecule. This type of interplay has been investigated by Zimmermann *et al.* in the paper mentioned above [6], although from a different point of view. If the "feedback" were absent, the Young-like picture would be perfectly adequate to describe the interference phenomenon, as shown in the case of the photoemission equivalent of the CF formula.

The same conclusion was reached by Baltenkov *et al.* [23] by comparing the interference pattern of Eq. (19) with the photoemission angular distribution of a model of two equivalent atoms scattering only in s waves, but sufficient enough to contain the effect of the feedback of one source onto the other.

The factor $[1 + \cos(\mathbf{k}\cdot\mathbf{R})]$ is the ubiquitous interference factor for coherent emission of two equivalent centers present in other spectroscopies. Notably, it is present in the case of "coherent electron emission from simple molecules by impact of energetic charged particle" [5]. In the case of heavy ion impact the key equation is given by Eq. (15) of the review paper by Ciappina *et al.* [5]

$$|\tilde{\mathbf{T}}_{fi}(\boldsymbol{\eta}, \boldsymbol{\rho})|^2 = \{1 + \cos[(\mathbf{k} - \mathbf{q})\cdot\boldsymbol{\rho}]\}|\tilde{\mathbf{T}}_{fi}(\boldsymbol{\eta})|^2,\tag{20}$$

where $\tilde{\mathbf{T}}_{fi}(\boldsymbol{\eta}, \boldsymbol{\rho})$ is the active electron scattering matrix element (AESME), $\boldsymbol{\eta}$ is the transverse part of the momentum $\mathbf{q} = \mathbf{K}_f - \mathbf{K}_i$ transferred by the impinging ion to the molecule, $\mathbf{k}$ is the wave vector of the ejected (active) molecular electron and $\boldsymbol{\rho}$ is the vector describing the orientation of the molecular axis. The decoupling between $\boldsymbol{\eta}$ and $\boldsymbol{\rho}$ in the AESME is achieved by means of the two effective center (TEC) approximation, which is done also in the case of electron impact. The analogies and differences with the Young's experiment have been studied mainly in conjunction with the interference factor $\{1 + \cos[(\mathbf{k} - \mathbf{q})\cdot\boldsymbol{\rho}]\}$ with the conclusion that analogies

should be taken with caution since the presence of **q** "may play a crucial role." This is probably in connection with the presence of the variable η in the effective one center matrix element $\tilde{\mathbf{T}}_{fi}(\boldsymbol{\eta})$, in line with our analysis.

C. Photoelectron diffraction along the molecular axis in N_2 and CO

Equation (18) is only an approximate form of the photoemission cross section in the case of homopolar molecules and was considered only for discussing its relation to other spectroscopies regarding the similarity to a Young's two-slit experiments.

In Appendix A 2 we derive the exact expression which we report in the main text for the convenience of the reader:

$$\frac{d\sigma}{d\hat{\mathbf{k}}} = 2\pi^2 \alpha \, \hbar\omega \left| \sum_L M_L^*(E) \left[(1 \pm e^{i\mathbf{k}\cdot\mathbf{R}}) A_L^{11}(\mathbf{k}) \right. \right.$$
$$\left. \left. + A_L^{12}(\mathbf{k}) \, e^{i\mathbf{k}\cdot\mathbf{R}} \pm (-1)^l A_L^{12}(-\mathbf{k}) \right] \right|^2, \quad (21)$$

where $A_L^{ij}(\mathbf{k}) = \sqrt{\frac{k}{\pi}} \sum_{L'} \tau_{LL'}^{ij} \, i^{l'} Y_{L'}(\hat{\mathbf{k}})$.

Based on this expression we have calculated the photoelectron diffraction intensity versus electron kinetic energy for electron emission along the molecular axis (assumed henceforth to coincide with the z direction of the laboratory frame) with photon polarization along the same direction, in the homonuclear molecule N_2 for the gerade ($+$) and ungerade ($-$) initial state, according to the experimental conditions chosen in Ref. [6]. The choice of the photon polarization along the molecular axis was taken to maximize the intramolecular scattering.

To compare with Fig. 4 of Ref. [6] we have summed the two cross sections in Eq. (21) corresponding to $\hat{\mathbf{k}} \cdot \hat{\mathbf{R}} = \pm 1$, since the emphasis in the selection of events [6] was on the

FIG. 2. Photoelectron diffraction intensity versus electron wave vector k expressed in units of R^{-1} for electron emission along the direction of the molecular axis with photon polarization along the same axis in the homonuclear molecule N_2. "PED$_g$" (full line) is for the gerade ($+$) state, "PED$_u$" (long-dashed line) for the ungerade ($-$) state. Experimental points are from Fig. 4 of Ref. [6]. The short-dashed curves represent the model used in Ref. [6] to interpret the data. See text for details.

"energy-resolved detection of the gerade and ungerade states rather than on the directional separation of forward and backward scattering events" along the molecular axis. The result is shown in Fig. 2 where the curve labeled "PED$_g$ (PED$_u$)" represents the PED intensity of the gerade ($+$) [ungerade ($-$)] channel. Their sum, given by the light blue (dot-dashed) curve, re-establishes the EXAFS periodicity of the diffracted intensity, since it is equivalent to a single center emission (see Fig. 4).

In the same figure we have reported the experimental points in Fig. 4 of Ref. [6] and have adopted their k units to make easier the comparison. (We have used the conversion: $k(\text{a.u.}^{-1}) = 0.529 \, k(R^{-1})/R$ to pass from our k units (a.u.$^{-1}$) to their units (R^{-1}), where $R = 1.1$ is in Å.) Henceforth, the notation $k(R^{-1})$ will indicate that k is measured in units of R^{-1}.

The short-dashed lines in Fig. 2 represent the model simulations adopted by the authors of Ref. [6], according to which the photoelectron diffraction intensities of the gerade and ungerade states were simulated by a superposition of two sine functions representing fractional intensities of the scattered (shown in their Fig. 5) and nonscattered electrons, respectively, in the spirit of a generalized Cohen-Fano model. It is an *ad hoc* model which however is at variance with the exact expression Eq. (21) [derived from Eq. (17) in Appendix A 2], where the interference function between the scattering amplitudes centered on the two sites is given by the phase difference $e^{i\mathbf{k}\cdot\mathbf{R}}$, as usual in quantum mechanics.

A comment is in order here on the normalization of the experimental data. The g/u data have been normalized to the corresponding absorption cross section $\sigma_{g/u}$ up to 4.7 $k(R^{-1})$. Afterward, the data have been normalized to $(\sigma_g + \sigma_u)/2$ to enhance the oscilatory behavior of the cross section. This renormalization explains why for $k(R^{-1}) < 4.7$ the experimental data do not show the typical shape resonance behavior in this region, whereas in the second region they do not show the typical decreasing behavior of the atomic cross section. Both features are evident in our theoretical 'raw' data which have been plotted whitout any treatment.

To understand the minima of the "PED$_{g/u}$" we use Eq. 21 and assume for sake of illustration that

$$A_L^{12}(\mathbf{k}) \approx (-1)^l A_L^{12}(-\mathbf{k}), \quad (22)$$

so that for the gerade and ungerade cross section we obtain

$$\frac{d\sigma_{g/u}}{d\hat{\mathbf{k}}} \propto \left| \sum_L M_L^*(E) \left[A_L^{11}(\mathbf{k}) \pm A_L^{12}(\mathbf{k}) \right] \right|^2 [1 \pm \cos(\mathbf{k}\cdot\mathbf{R})]. \quad (23)$$

Therefore, we expect minima for the gerade and ungerade cross section at $kR = n\pi$ with n odd or even, respectively. This is in fact what one roughly finds due to the approximation (22). The first experimental [and theoretical within 0.15 (R^{-1})] minimum of the ungerade state falls at $k = 5.2(R^{-1})$ so that $kR = 1.7\pi$, while the second theoretical minimum falls at $k = 11.7(R^{-1})$ giving $kR = 3.7\pi$. For the gerade state we find the experimental [and theoretical within 0.15 (R^{-1})] at $k = 8.5(R^{-1})$ so that $kR = 2.7\pi$, whereas the second theoretical minimum falls at $k = 15.0(R^{-1})$ giving $kR = 4.8\pi$ The
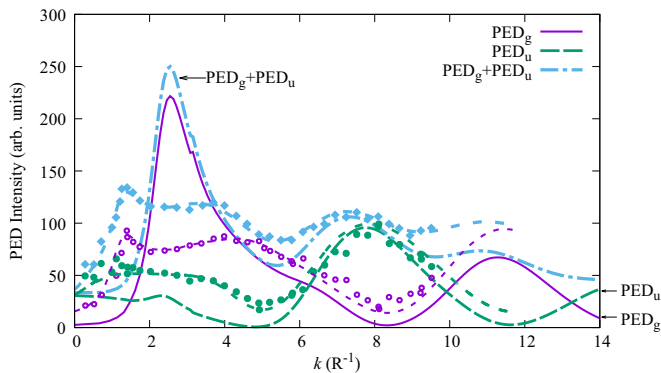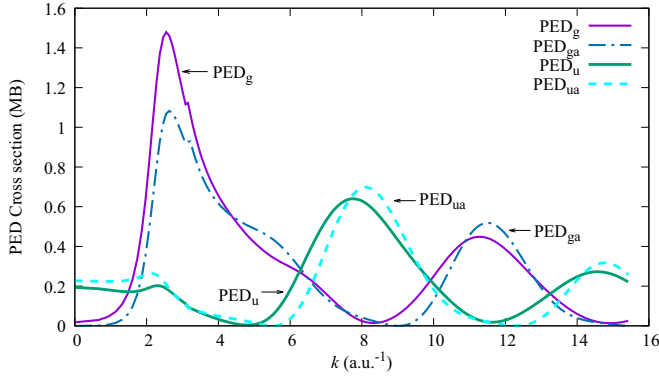
FIG. 3. Comparison between the exact expression Eq. (21) and its approximation Eq. (23). The labels "PED$_{ga}$" (dot-dashed line) and "PED$_{ua}$" (dashed line) indicate the approximate cross sections

FIG. 4. PED intensity for the "forward" (full line) and "backward" (dashed line) channels in the N_2 molecule, obtained from a calculation that artificially suppresses the contribution of one of the two emitting centers. Photon polarization along the molecular axis.

deviation from the condition of exact zeros in the interference factor is of the order of 0.2–0.3π, which shows that the approximation (22) is reasonable. This is confirmed by Fig. 3 which shows the comparison between the exact expression Eq. (21) and its approximation Eq. (23)

A second important point to underline is the fact that the shape resonance in the ungerade cross section is depressed compared to the gerade one. This can be explained by looking at Eq. (23), since the two amplitudes $A_L^{11}(\mathbf{k})$ and $A_L^{12}(\mathbf{k})$ interfere constructively in the gerade case and destructively in the ungerade one. We shall discuss further this point below in Sec. IV C.

Figure 4 shows the result of a calculation (a theoretical experiment!) for the N_2 molecule that artificially suppresses the contribution of one of the two centers. This is obtained by suppressing the terms immediately following the $\pm$ sign in Eq. (21) and multiplying the cross section by two, or equivalently by using Eq. (17) with $c_1 = 1$ and $c_2 = 0$. In the calculations the emitter is the atom located at $(0, 0, -R/2)$. The curve labeled by "PED$_{+1}$" plots the PED intensity of the "forward" channel [6], (emission into the molecule, therefore $\hat{\mathbf{k}} \cdot \hat{\mathbf{R}} = 1$), whereas the curve labeled "PED$_{-1}$" represents the "backward" channel (emission out of the molecule, therefore $\hat{\mathbf{k}} \cdot \hat{\mathbf{R}} = -1$). Their sum is given by the blue curve. The resulting behavior is similar to Fig. 2 of Ref. [6], which however represents the carbon K-edge absorption of the CO molecule. The similarity confirms that the important physical process is the emission from a single site. One can easily understand the different behavior of the two channels in the high energy region by making the single scattering approximation for $\boldsymbol{\tau} \approx T + TGT + \cdots$ in the expression (A4). In this way the scattering amplitude $B_L^c(\mathbf{k})$ for the photoabsorber becomes (for an initial $l = 0$ state), dropping the site indication,

$$B_1(\mathbf{k}) \propto t_1 \left[(\mathbf{e} \cdot \hat{\mathbf{k}}) + (\mathbf{e} \cdot \hat{\mathbf{R}}) f_{\text{eff}}(\hat{\mathbf{k}} \cdot \hat{\mathbf{R}}) \frac{e^{ikR(1-\hat{\mathbf{k}}\cdot\hat{\mathbf{R}})}}{kR} \right], \quad (24)$$

where $\mathbf{e}$ is again the photon polarization, $\mathbf{R}$ is the vector joining the photoabsorber with the other atom, $f_{\text{eff}}(\hat{\mathbf{k}} \cdot \hat{\mathbf{R}}) = \sum_l (2l + 1) t_l P_l(\hat{\mathbf{k}} \cdot \hat{\mathbf{R}}) g_{1l}(kR)$ is an effective scattering amplitude and $g_{1l}(kR)$ is the curved wave correction of the free propagator G in Eq. (A6). This is the well known single
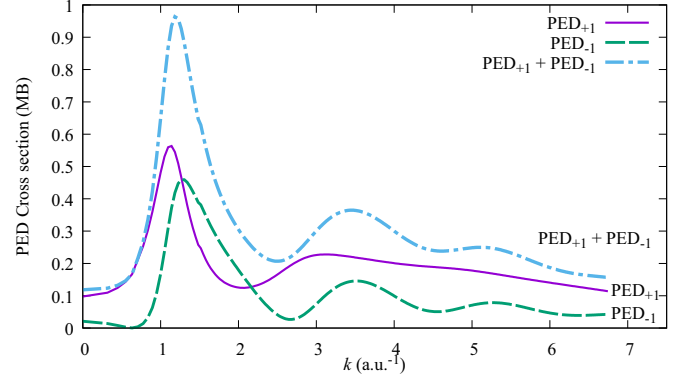
scattering expression for PED [25]. We see that for $\hat{\mathbf{k}} \cdot \hat{\mathbf{R}} = 1$ the exponent of the propagator is zero, leading to a flat behavior of the PED cross section, whereas $\hat{\mathbf{k}} \cdot \hat{\mathbf{R}} = -1$ leads to the typical EXAFS oscillation with period $\Delta k = \pi/R$.

For completeness, we also give in Fig. 5 the PED spectrum for the CO molecule together with the experimental points taken from Fig. 2 of Ref. [6]. In the words of the authors, "all diffraction intensities have been normalized to the corresponding partial cross-sections to remove the exponential decay behavior, which would otherwise mask the oscillatory structure." Again the theoretical data have not been treated, so that they show after $k = 4.7\,(R^{-1})$ the typical decreasing behavior of the atomic cross section. It is not clear what is the "corresponding partial cross section." In Fig. 6 we give the theoretical cross sections renormalized by $M_L^*(E) A_L^{11}(\mathbf{k})$. The effect of leveling of the cross section is reproduced after $k = 4.7\,(R^{-1})$, but below this value of k there seems to be a problem of normalization.

Coherence effects in N_2 are also observed in the angular distribution of the emitted photoelectrons as opposed to the localized emission case. Our results are the same as those
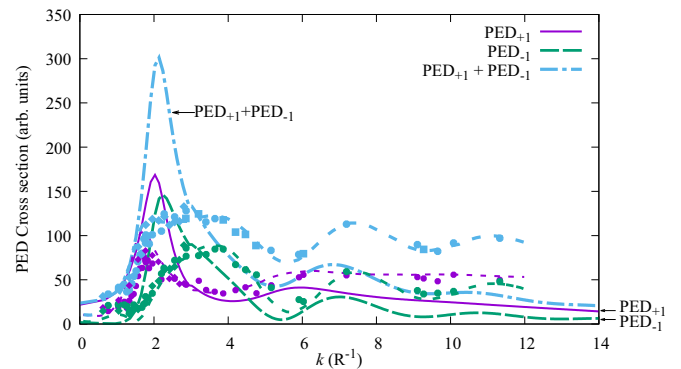

FIG. 5. PED intensity for the "forward" and "backward" channels in the CO molecule together with the experimental points taken from Ref. [6]. Photon polarization along the molecular axis. Same line conventions as in Fig. 2 .
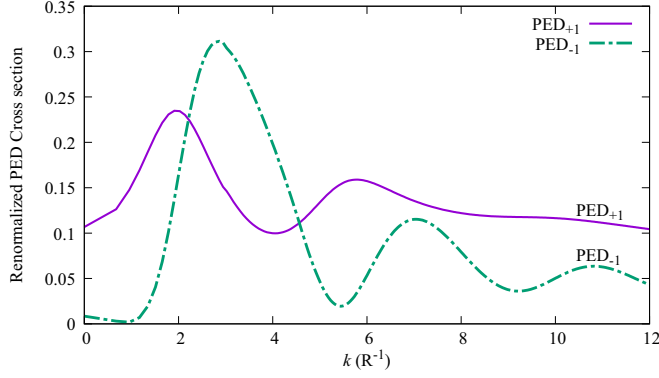
FIG. 6. CO renormalized PED spectra: Photoemission along molecular $+/-z$ axis. Photon polarization along positive z axis.

obtained in Sec. 5.2 of Ref. [4] by the MS approach with non spherical potentials. Therefore, they are not presented here.

In the PED calculations of the CO spectra (as in the absorption spectrum below) we have used a complex HL potential just to show that its role is to dampen a bit the effects of coherent interference, as anticipated above.

IV. PHOTOABSORPTION FROM DIATOMIC MOLECULES

The relation $\int d\hat{\mathbf{k}} \cos(\mathbf{k} \cdot \mathbf{R}) = 4\pi \sin(kR)/(kR)$ prompted some authors [26] to derive the Cohen-Fano formula [1] by integrating Eq. (18) over the directions of the photoelectron momentum $\hat{\mathbf{k}}$, after averaging over the molecular orientations to calculate the unpolarized absorption cross section. However, the resulting expression could only be approximate due to the simultaneous $\mathbf{k}$ dependence of the PED cross section and the interference term. More physical insight could be gained by calculating directly and exactly the polarization-dependent photoabsorption cross section.

Starting from the initial state Eq. (15), integrating Eq. (12) over $d\hat{\mathbf{k}}$ and using Eq. (10) we find, neglecting again the contribution of the outer cell Ω_3,

$$\sigma_{\text{abs}}(\omega) = -4\pi\,\alpha\,\hbar\,\omega \left[\sum_i^{1,2} c_i^2 \sum_{LL'} M_L^i(E)\Im\tau_{LL'}^{ii}(M_{L'}^i)^{\star}(E) \right.$$
$$\left. + \sum_{i \neq j}^{1,2} c_i c_j \sum_{LL'} M_L^i(E)\Im\tau_{LL'}^{ij}(M_{L'}^j)^{\star}(E) \right] \quad (25)$$

due to the symmetry $\tau_{LL'}^{ij} = \tau_{L'L}^{ji}$ holding in real spherical harmonic basis. Note that the integration over $d\hat{\mathbf{k}}$ has restored the equivalence over the two sites.

To illustrate the effect of the photon polarization, Fig. 7 gives the CO absorption cross section from a 1σ carbon initial state (in the limit $c_2 \to 0$) both for photon polarization along the molecular z axis and orthogonal to it. As expected, the shape resonance and the EXAFS oscillations appear only in the first case. When the photoelectron is ejected in the (x, y) direction no such effects are observed due to the absence of back-scattering atoms. The curves with line points represent the same cross sections calculated in the velocity gauge.

FIG. 7. The CO absorption spectrum from a 1σ carbon initial state with photon polarization along the molecular z axis and perpendicular to it. In this latter case no oscillations of the cross section are observed due to the absence of back-scattering atoms. The curves with line points represent the same cross sections calculated in the velocity gauge.
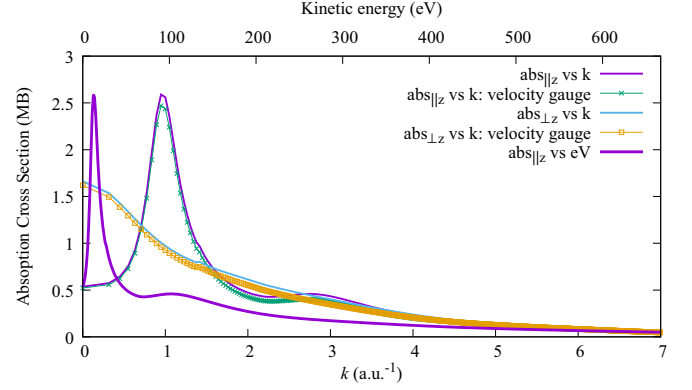
If we assume an initial state of the type $\sigma_{g,u}$,

$$\phi_{g,u}(\mathbf{r}) = \frac{1}{\sqrt{2}}[\phi(\mathbf{r}_1) \pm \phi(\mathbf{r}_2)], \quad (26)$$

then Eq. (25) reduces to

$$\sigma_{abs}(\omega) = -4\pi\,\alpha\,\hbar\,\omega\left[\sum_{LL'} M_L(E)\Im\tau_{LL'}^{11}M_{L'}^{\star}(E) \right.$$
$$\left. \pm \sum_{LL'} M_L(E)\Im\tau_{LL'}^{12}M_{L'}^{\star}(E) \right]. \quad (27)$$

A. Photoabsorption in homopolar diatomic molecules: The Cohen-Fano interference term revisited

In the independent particle approximation, Eq. (27) is the exact expression for the total absorption cross section of the molecule. It consists of two terms, the first of which is the usual term describing processes in which the emitting atom acts also as a detector, measuring the interference between the outgoing and the incoming photoelectron wave and leading to EXAFS-like oscillations in the cross section with maximum k period of $\Delta k = 2\pi/2R = \pi/R$. The second term instead describes processes where one atom acts as the emitter and the other as the detector (and viceversa), generating oscillations in the cross section with maximum period $\Delta k = 2\pi/R$. This is the lowest order feature of other higher-order oscillations of this type present in the absorption cross section with period $\Delta k = 2\pi/nR$, where n is any odd integer number. However, their intensity fades away quite rapidly with increasing photoelectron energy and since they add incoherently with increasing frequency they constitute a featureless background which is eliminated in data analysis. Therefore, only the biggest $n = 1$ signal survives, which is the CF oscillation (see discussion below in Sec. IV B).

To make contact with Cohen-Fano's assumptions in deriving their expression, we work in the Born approximation, use the muffin-tin approximation for the atomic scattering amplitudes ($T_{LL'} \approx t_l\delta_{LL'} = -1/k\,e^{i\delta_l}\sin\delta_l$), where δ_l is the l_{th}

phase shift of the spherically averaged atomic potential, and assume initial $\phi_{1s}(\mathbf{r}_i)$ orbitals, so that only an $l = 1$ final state is selected by the dipole transition matrix element.

In the Born approximation, according to Eq. (A4) in Appendix A 1, $\boldsymbol{\tau}_{LL'}^{ii} \approx t_l \, \delta_{LL'}$ and $\boldsymbol{\tau}_{LL'}^{12} \approx t_l G_{LL}^{12} t_{l'} \, \delta_{LL'}$. To get more insight into the derivation of the CF formula, we treat separately the cases of longitudinal and perpendicular polarization with respect to the molecular axis. For z polarization the atomic matrix element M_L selects the $L = (10)$ final orbital state, so that, using the approximation (A6) for the free spherical wave propagator, Eq. (27) yields

$$\sigma_{\mathrm{abs}} \approx \sigma_{\mathrm{at}} \left\{ 1 \, \pm \, 3A_{11}(kR) \, \frac{\sin[kR + 2\delta_1 + \phi_{11}(kR)]}{kR} \right\}, \quad (28)$$

where $\sigma_{\mathrm{at}} = 4 \pi \alpha \hbar \omega |M_1|^2 / k \, \sin^2 \delta_1$ is the atomic absorption. As in Ref. [1] we have taken $\mathbf{R}_{ij}$ along the z axis so that $|Y_{10}(\hat{\mathbf{R}}_{ij})|^2 = 3/(4\pi)$. which entails the factor of three in Eq. (28). For the perpendicular polarization, since $|Y_{11}(\hat{\mathbf{R}}_{ij})|^2 = 0$, we find only the atomic absorption and no oscillatory term in Eq. (28). Figure 7 clearly illustrates this point in the case of CO photoabsorption. As a consequence the unpolarized cross section re-establishes the CF result with the factor one in front of the oscillatory term. Since summing over the photon polarizations is equivalent to averaging over the molecular orientations, very often authors in the literature make use of this second method in discussing the application of the CF formula. However, there are configurational averages that do lead to a CF functional form, but do not have the same physical meaning. We defer the discussion of this point to the end of Sec. V.

The additional amplitude $A_{11}(kR)$ and phase $\phi_{11}(kR)$ in Eq. (28) originate from the function $g_{ll'}^0(kR)$ in Eq. (A7). Their expressions for $l = l' = 1$ are $\phi_{11}(kR) = 2/(kR)$ and $A_{11}(kR) = [1 + 2/(kR)^2]^{1/2} J_0[4/(kR)^2]$.

The phase shift $2\delta_1$ has the same origin as for the EXAFS term and was also found by Liu *et al.* [26] who took into account MS within the molecule. It was missed by Cohen and Fano due to their simplifying assumption of a final plane wave photoemission state. Together with the phase ϕ_{11}, it can be important in the determination of the bond length since it might not be negligible. Their neglect is responsible for the fact that the bond lengths of N_2 and O_2 molecules, measured in photoabsorption from delocalized valence states, were found shorter than the equilibrium ones [16], as shown below.

A further comment is in order here, regarding the physical meaning of the Cohen-Fano interference term. As apparent from the second term of Eq. (27) and the Born approximation of the full scattering path operator $\tau_{LL'}^{12}$, it is clear that the interference term stems from the imaginary part of the free electron propagator $G_{LL'}^{12} \approx e^{ikR_{12}}/(kR_{12})$, reinforcing the picture of site 1 as the source of the photoelectron and of site 2 as the detector (or viceversa).

This is physically different from the Young two-slit experiment, where both slits act as sources of the interfering (photon or electron) waves. Rather, the similar polarization dependence of the EXAFS and CF oscillations and the appearance
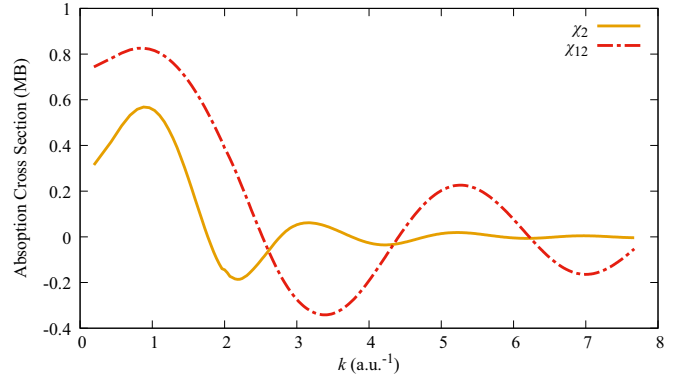

FIG. 8. The EXAFS χ_2 (full line) and CF interference term χ_{12} (dot-dashed line) in N_2 absorption spectrum normalized to the atomic absorption σ_{at} for polarization along the molecular axis.

of the atomic phase shifts in the sinus argument characterizes the corresponding oscillations as the remnants of the PED patterns on the energy scale, after averaging over the emission angles. In the case of EXAFS they are associated to closed paths beginning and ending at the same atom, whereas in the case of the CF signal they are associated to open paths going from one photoabsorber to the other, acting as source and detector of the photoelectron, respectively.

B. The validity of the Born Approximation: Application to the oscillatory structure of the N_2 valence photoabsorption ionization cross section

To see the region of validity of the Born approximation we have calculated the spectral radius $\rho(\mathbf{TG})$ of the matrix $\mathbf{TG}$, while calculating the N_2 full potential absorption. Already at 100 eV of the photoelectron kinetic energy (corresponding to $k \approx 2.7$ a.u.$^{-1}$), $\rho \approx 1/4$, so that we can stop the series expansion at $n = 2$ in Eq. (A3). $\boldsymbol{\tau} \approx \mathbf{T} + \mathbf{TGT} + \mathbf{T(GT)}^2$.

Figure 8 plots two curves χ_2 and χ_{12} as a function of k (a.u.$^{-1}$) from $k = 0$, where $\chi_2 = [M^1(E)]^2 \Im (T^1 G^{12} T G^{21} T^1)/\sigma_{\mathrm{at}} - 1$ is the usual EXAFS signal in structural analysis and $\chi_{12} = [M^1(E)]^2 \Im (T^1 G^{12} T^2)/\sigma_{\mathrm{at}}$ is the CF signal, both normalized to the atomic absorption $\sigma_{\mathrm{at}} = M_L^n(E) \Im T_{LL}^n M_L^n(E)$ ($n = 1$ or 2) for $l = 1$.

We see that the χ_{12} CF term is dominant in all k range compared to the χ_2 EXAFS signal. This is in keeping with the ordering of the paths described in Appendix A 1. The next CF signal comes from the term $n = 3$ in the series expansion of $\boldsymbol{\tau}: \Im (T G^{12} T G^{21} T G^{12} T)$. However, the frequency of this signal is three times that of the CF signal and its amplitude is similar the EXAFS signal, i.e., roughly ten times smaller than the first term. The presence of higher-order oscillations, out of phase of each other, will form a featureless background which is eliminated in the data analysis. The dominance of χ_{12} at high energy had been noted before [5].

The period of the CF oscillation is $\Delta k = 2\pi/R_{\mathrm{eff}} = 6.95 - 3.40 = 3.55$ a.u.$^{-1}$, corresponding to an effective bond length $R_{\mathrm{eff}} = 0.94$ Å, the same as that derived from the fitting procedure used in Ref. [16].

Figure 9 shows the comparison of our *ab initio* calculated CF $\chi_{12}(k)$ signal with the experimental points presented in Ref. [16].
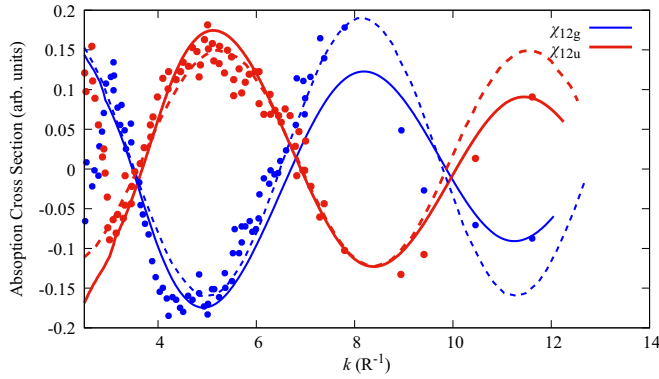
FIG. 9. Comparison of the calculated CF signal (full lines) with experimental points and the fitted CF signal (dashed lines) of Ref. [16].

The k axis is now in (R^{-1}) (with R in Å). Before making the change of units, the "χ_{12g}" curve was shifted by -1.2 (a.u.$^{-1}$) and the "χ_{12u}" curve by -1.0 (a.u.$^{-1}$) due to the fact that the ionization threshold of our potential does not coincide with the experimental one and the two initial edges are slightly different (respectively, $3\sigma_g$ and $1\pi_u$).

The authors in Ref. [16] interpreted this value of R_{eff} as an indication that "a delocalized valence state has a smaller effective bond length compared to the equilibrium bond lengths." However, before reaching any conclusion one should correct this value by $-2a$, where $-a$ is the coefficient of the linear term in the fit of the total phase shift $\delta_1 + \phi_{11} = -ak + b$, which is shown in Fig. 10. We find a $= 0.08$ Å, so that $R_{\text{corr}} = 0.94 + 0.16 = 1.1$ Å.

Since the valence states are mainly composed of their respective atomic $p(l = 1)$ and $s(l = 0)$ states, the emitted photoelectrons have predominantly $p(l = 1)$ and $d(l = 2)$ character. Figure 10 shows the corresponding phase shifts. Both δ_1 and $\delta_2 + \phi_{22}$ have the same slope $a = 0.06$, so that there is enough indication that the true bond length is the equilibrium one. Unfortunately the error in the determination of R_{eff} was not given in Ref. [16]. We note here the importance of the curved wave phase ϕ_{ll} correction, especially important for the δ_2 atomic phase shift, which is almost flat in the asymptotic region $7 < k < 16$.
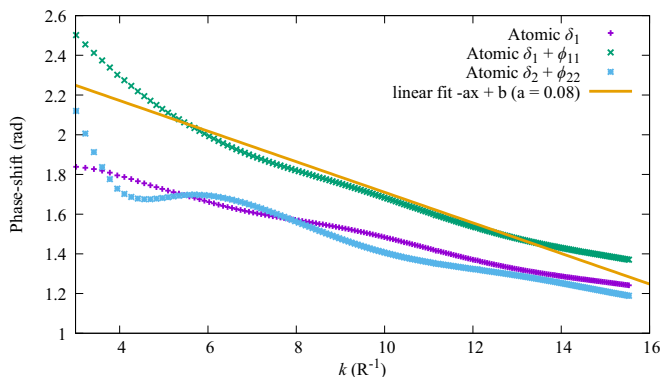

FIG. 10. Linear fit of the total $\delta_1 + \phi_{11}$ phase shift. Also shown is $\delta_2 + \phi_{22}$ and δ_1 alone.
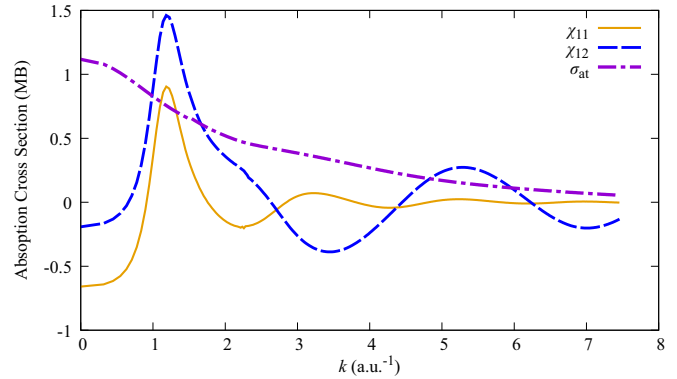

FIG. 11. Plot of full single site absorption $\propto \Im\tau^{11}$ (χ_{11}; full line) and the CF signal $\propto \Im\tau^{12}$ (χ_{12}; dashed line) of Eq. (27) for the gerade state σ_g and photon polarization along the molecular axis in the whole k-range divided by the atomic absorption. The atomic absorption (σ_{at}; dot-dashed line), independent of the photon polarization, is also shown.

C. Analysis of the photoabsorption cross section in the whole spectral range

Figure 8 shows the behavior of χ_2 and χ_{12} from $k = 0$. However, their validity is restrained only to the region $k \geqslant \approx 2.7$ a.u.$^{-1}$, since at lower energies other contributions are present, coming from higher-order MS paths which in this region have bigger amplitudes due to the low value of k. Moreover, these paths can interfere constructively like in the case of the shape resonance at 18 eV in N_2, enhancing the cross section. In Fig. 11 we plot separately the corresponding quantities (proportional, respectively, to $\Im\tau^{11}$ and $\Im\tau^{12}$ in Eq. (27), again for the gerade state) obtained by inverting exactly the MS matrix in the whole energy range. We see that for $k > 2.7$ a.u.$^{-1}$ they practically coincide with the results obtained by calculating τ by series expansion, whereas they show the typical shape resonance behavior around 18 eV. For reference, the atomic absorption σ_{at} is also shown. The total cross section is the sum of all three curves, after multiplying the first two oscillatory signals by σ_{at}.

While in the region around the shape resonance the single site absorption and the CF signal for the gerade initial state interfere constructively, one expects the opposite for the ungerade initial state, so that the shape resonance in this last case should almost disappear. This is what is observed in Fig. 12, which plots the total absorption cross section for the gerade σ_g and ungerade state σ_u divided by the atomic cross section σ_{at}.

This result for N_2 was in fact already known to the authors of Ref. [27], who used MS theory to derive it, but without providing any comment that could give a physical explanation for this finding. However, a flat cross section for the σ_u channel in the region of the shape resonance is in disagreement with the experimental angular distributions of photoelectrons ejected from fixed-in-space N_2 molecules, which could be reproduced theoretically only after taking into account many-electron correlations using the random phase approximation (RPA) method [28]. The ratio $\sigma_g(\omega)/\sigma_u(\omega)$ was later calculated in the RPA by Semenov *et al.* [29] who
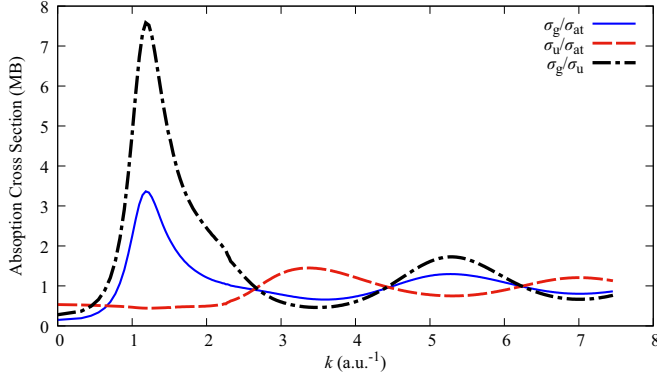
FIG. 12. Plot of total absorption cross for the gerade σ_g (full line) and ungerade σ_u (dashed line) initial state and their ratio (dot-dashed line). Photon polarization along the molecular axis

found a maximum ratio of 1.8, which is in agreement with the same ratio seen experimentally in Fig. 2 for photoemission.

Indeed, our approach can only describe the independent particle aspect of the interaction and cannot describe the many body aspect of the excitation process. It is asymptotically correct above 50–100 eV of photoelectron kinetic energy (depending on the systems) since then the electron-electron interaction plays a marginal role that can be accounted for by an absorptive complex potential and interchannel coupling is ineffective.

D. Cooper-like minima and electron confinement

It is known that the total photoabsorption cross section $\sigma_{tot}(\omega)$ can be decomposed in partial cross sections (PCS) $\sigma_l(\omega)$, each one in correspondence with an l partial wave of the final state wave function $\psi_{\mathbf{k}}^-(\mathbf{r})$, so that $\sigma_{tot}(\omega) = \sum_l \sigma_l(\omega)$, the final angular momentum l being an odd integer due to the dipole selection rule. These PCS exhibit deep minima when the relation $kR = l\pi$ is approximately satisfied. These interference effects have been related to a confinement effect of the ejected photoelectron [17]. Later work by the authors in Ref. [24] related these minima to CF modulations considering them as "Cooper-like minima." They actually found this connection somewhat puzzling, since Cooper minima appear in the photoelectron spectra of homonuclear and heteronuclear molecular targets [30] while CF modulations "appear only in the case of homonuclear molecules" (at the time of writing it was not yet known that CF oscillation could be present also in heteronuclear molecules, like CO [8]!).

In Appendix A 3 we calculate the PCS using our MS approach. The result [changing l to λ and omitting for simplicity the global parity factor $P_f = 1 - (-1)^{\lambda-1}$] is

$$\sigma_\lambda(\omega) \propto \sum_{m_\gamma m_\lambda} \sigma_{m_\gamma}^{at}(\omega) \left| |A_\lambda| e^{i\phi_\lambda} + \frac{e^{ikR}}{kR} |B_\lambda| e^{i\psi_\lambda} \right|^2$$

$$\propto \sum_{m_\gamma m_\lambda} \sigma_{m_\gamma}^{at}(\omega) \left[|A_\lambda|^2 + \frac{|B_\lambda|^2}{(kR)^2} \right.$$

$$\left. + 2 |A_\lambda||B_\lambda| \frac{\cos(kR + \eta_\lambda)}{kR} \right], \quad (29)$$

where A_λ and B_λ are complex amplitudes defined in Eqs. (A18) and (A19) in terms of $\tau^{ii}(i = 1, 2)$, respectively, and $e^{ikR}/(kR)$ comes from the free propagator G^{12} of Eq. (A6).

Minima of this expression occur at energies such that $kR + \eta_\lambda = n\pi$, with n odd integer, where $\eta_\lambda = \psi_\lambda - \phi_\lambda$. Note however that for each partial cross section $\sigma_\lambda(\omega)$ there are several such minima, as found for example by Semenov *et al.* [29] for the N_2 molecule. Equation (29) is consistent with the connection between CF modulations and Cooper-like minima considered in Ref. [24]. Indeed, the CF oscillations are related to $\Im G^{12}$ due to the generalized optical theorem valid for total photoabsorption, while for the PCS one has to consider amplitudes squared. Clearly there is no mechanism for electron confinement.

The extension of this result to heteropolar molecules is straightforward, so that, depending of the mixing coefficients c_1 and c_2 in Eq. (15) one can expect to observe Cooper-like minima also in these molecules

E. Photoabsorption in heteropolar diatomic molecules

If we use again the Born approximation for τ in Eq. (25) and assume a main transition to a final l state, we find a result very similar to the homopolar case for the unpolarized cross section:

$$\sigma_{abs} \approx \sum_i^{1,2} c_i^2 \sigma_{at}^i + 2 c_1 c_2 A_{ll}(kR)$$

$$\times \frac{\sin\left[kR + \delta_l^1 + \delta_l^2 + \phi_{ll}(kR)\right]}{kR} \sqrt{\sigma_{at}^1} \sqrt{\sigma_{at}^2}, \quad (30)$$

where $\sigma_{at}^i = 4\pi\alpha\hbar\omega |M_l^i|^2/k \sin^2 \delta_l^i$ and $R = R_{ij}$. This behavior with periodicity $2\pi/R$ has been found experimentally in the vibrationally resolved photoionization of the $1\pi^{-1}$ valence state of the heteropolar molecule CO in Ref. [8]. In this case the $\phi_i(\mathbf{r}_i)$ orbitals are approximately $2p$ Carbon and Oxygen atomic states, so that the main orbital transition is to $l = 2$. In this case $\phi_{ll} = 6/(kR)$ and $A_{ll}(kR) = [1 + 6/(kR)]^{1/2} J_0[36/(kR)^2]$.

Equation (30) shows that a Cohen-Fano interference term is also present in the photoionization of heteropolar diatomic molecules like CO. However, its experimental observation depends critically on the value of the product $c_1 c_2$. For the 1σ initial state we estimate this product to be of the order of $t/\Delta E_{12}$, where $t \approx 0.05$ eV is the resonance integral (equivalent to the hopping integral in band theory) between the carbon and oxygen sites and $\Delta E_{12} \approx 250$ eV is the energy difference between the energies of the respective atomic $1s$ orbitals. Therefore, $c_1 c_2 \approx 2 \times 10^{-4}$, which makes the CF oscillations practically undetectable. The reason however is the smallness of the product $c_1 c_2$ rather than the inequivalence of the two atomic sites.

In the case of the photoabsorption of the $1\pi^{-1}$ valence state instead, assuming the approximate values for $c_1^2 = 0.68$ and $c_2^2 = 0.32$ suggested in Ref. [8], we obtain $c_1 c_2 = 0.47$, which implies the possibility of a direct experimental detection of the CF oscillations in photoabsorption. Similar coefficients are found for the 3σ valence state.

V. ELASTIC ELECTRON-MOLECULE SCATTERING

In the light of the coherence concept, it is worth pointing out that another spectroscopy can give access to CF oscillations. This is the orientationally averaged scattering of electrons off small molecules, in particular diatomic molecules.

The related integrated cross section has been given by Dill and Dehmer [31] as

$$\sigma_{\text{AES}}(E) = 4\pi \sum_{LL'} |T_{LL'}|^2, \tag{31}$$

where E is the energy of the impinging electron beam with wave number $k = \sqrt{E}$ and $T_{LL'}$ is the scattering matrix of the molecule.

In the framework of MST, indicating by o the molecular center (origin of the coordinates), $T_{LL'}$ is given by [9]

$$T_{LL'} = \sum_{ij} \sum_{\Lambda \Lambda'} J_{L\Lambda}^{oi} \tau_{\Lambda\Lambda'}^{ij} J_{\Lambda'L'}^{jo}, \tag{32}$$

where $J_{LL'}^{oi}$ is the translation operator (TO) in MST given by

$$J_{LL'}^{oi} = 4\pi \sum_{L''} i^{l-l'+l''} C_{LL'}^{L''} J_{L''}(\mathbf{R}_{oi}), \tag{33}$$

where $J_L(\mathbf{R}) = j_l(kR) Y_L(\hat{\mathbf{R}})$, $j_l(kR)$ is the spherical Bessel function of order l and $C_{LL'}^{L''}$ is the usual Gaunt coefficient. This is reminiscent of the similar definition for the free spherical wave propagator (A5). Since $-ih_l^+(kR) = n_l(kR) - ij_l(kR)$, where $n_l(kR)$ is the Neumann function, we find the useful relation [32]

$$G_{LL'}^{oi} = k N_{LL'}^{oi} - i k J_{LL'}^{oi}, \tag{34}$$

where $N_{LL'}^{oi}$ has the same definition as $J_{LL'}^{oi}$ in Eq. (33), with the Neumann function replacing the Bessel function. Retaining for simplicity only the phase correction, Eq. (A6) entails therefore the following approximation for $J_{LL'}^{ij}$,

$$J_{LL'}^{ij} \approx -4\pi \frac{\sin[kR_{ij} + \phi_{ll'}(kR_{ij})]}{kR_{ij}} Y_L(\hat{\mathbf{R}}_{ij}) Y_{L'}(\hat{\mathbf{R}}_{ij}) i^{(l-l')}, \tag{35}$$

where $\phi_{ll'}(kR) = [l(l+1) + l'(l'+1)]/(2kR)$. Exact, useful properties of the TO are (see Appendix A of Ref. [32])

$$\sum_{L''} J_{LL''}^{oi} J_{L''L'}^{ij} = J_{LL'}^{oj}; \quad J_{LL'}^{oi} = J_{L'L}^{io}; \quad J_{LL'}^{ii} = \delta_{LL'}. \tag{36}$$

By application of the generalized optical theorem we find

$$\sum_{LL'} |T_{LL'}|^2 = \sum_{LL'} T_{LL'} T_{L'L}^* = -\frac{1}{k} \sum_L \Im T_{LL}, \tag{37}$$

remembering the symmetry property $T_{LL'} = T_{L'L}$. Therefore, we can write the cross section $\sigma_{\text{AES}}(E)$ as

$$\sigma_{\text{AES}}(E) = -\frac{4\pi}{k} \sum_{ij} \sum_{LL'} \Im(J_{LL'}^{ji} \tau_{LL'}^{ij}). \tag{38}$$

Specializing to a diatomic molecule and in the Born approximation of the scattering path operator τ used for arriving at

Eq. (28), we find

$$\sigma_{\text{AES}}(E) = \sigma_{\text{AES}}^1(E) + \sigma_{\text{AES}}^2(E) + 2\frac{4\pi}{k^2} \sum_{ll'} (2l+1)$$

$$\times (2l'+1) \sin\delta_l^1 \sin\delta_{l'}^2 \frac{\sin[kR + \phi_{ll'}(kR)]}{kR}$$

$$\times \frac{\sin[kR + \delta_l^1 + \delta_{l'}^2 + \phi_{ll'}(kR)]}{kR}, \tag{39}$$

taking into account that

$$-\frac{4\pi}{k} \sum_{LL'} J_{LL'}^{ii} \Im t_l^i = 4\pi \sum_l (2l+1) |t_l^i|^2 = \sigma_{\text{AES}}^i(E) \tag{40}$$

is the atomic scattering cross section and

$$4\pi \sum_L Y_L(\hat{\mathbf{R}}_{ij}) Y_L(\hat{\mathbf{R}}_{ij}) = \sum_l (2l+1) P_l(1). \tag{41}$$

In contrast to the photoemission case, the double sum over l, l' in Eq. (39) reflects the absence of a dipole selection rule, whereas the presence of the extra term $\sin(kR + \phi_{ll'})/(kR)$, originating from the TO, is due to the lack of selectivity of the electron probe in the scattering process, as apparent from the expression (38). However, the appearance of the CF term is related, like in photoemission, to the coherence of the "initial" electron state.

Similar phenomena of coherent electron emission from simple molecules have been observed in impacts of energetic charged particle [5].

It is interesting at this point to try to clarify the relation between averaging over the molecular orientations and the CF modulation factor. At the end of their paper [1], Cohen and Fano mention that their two-center modulation factor $[1 + \sin(kR)/(kR)]$ appears also in the formulas for elastic coherent scattering of x rays, electrons, or neutrons by a diatomic molecule [33]. We give here a short derivation of these formulas for the convenience of the reader and restrict for the sake of discussion to electron molecular scattering. Referring to Eq. (XIX.153) of Ref. [34], the amplitude for elastic electron scattering off an homopolar diatomic molecule fixed in space, is given to the lowest order of approximation by

$$\langle k|T|k_0\rangle \approx (1 + e^{-i\mathbf{q}\cdot\mathbf{R}}) \langle k|t|k_0\rangle, \tag{42}$$

where T is the transition matrix for the molecular scattering, t is the transition matrix for the single atomic scattering, $\mathbf{q} = \mathbf{k} - \mathbf{k}_0$ is the momentum transfer of the process, and $\mathbf{R}$ is the interatomic distance. This formula corresponds to the approximation $T \approx t_1 + t_2$ and neglects higher-order terms describing electron propagation from one site to the other, like $t_1 G t_2$. Therefore, for the transition probability we find

$$|\langle k|T|k_0\rangle|^2 \propto |\langle k|t|k_0\rangle|^2 [1 + \cos(\mathbf{q} \cdot \mathbf{R})], \tag{43}$$

which is the usual formula for this kind of interference. For scattering off a gas phase, one should average over the molecular orientations, obtaining

$$|\langle k|T|k_0\rangle|^2 \propto |\langle k|t|k_0\rangle|^2 \left[1 + \frac{\sin(qR)}{qR}\right], \tag{44}$$

since $\langle k|t|k_0\rangle$ depends only on the scattering angle. Clearly the functional form $[1 + \sin(qR)/(qR)]$ does not have the same physical origin as the CF interference found in

photoabsorption. Even though the original result [1] was found by averaging over the photon polarization (equivalent therefore to a configurational averaging) the same functional form was also found for the polarized CF signal, as shown by Eq. (28) of Sec. IV A, where it was associated to a MS path joining the two molecular centers. We might call this latter signal an *intrinsic* two-center modulation factor, as opposed to an *extrinsic* one, coming from a truly configurational average of the system under study. In this respect the signal obtained in Eq. (39) is of the *intrinsic* type, despite the configurational averaging, since it corresponds to a true propagation of the impinging electron from one site to the other of the molecule, due to the term $t_1 G t_2$, which was not neglected.

VI. CONCLUSIONS

Working in the framework of MS theory, we have shown that when the initial state in a photoemission process is extended over many atomic sites, whether equivalent or not, new MS processes are generated compared to the case of emission from a single localized site, due to the fact that emission from different sites is coherent, as dictated by the Feynman's rules [19]. In photoabsorption, these processes are characterized by the fact that the emitter does not coincide with the detector, as in the case of a localized emitter (where EXAFS type of oscillations are generated in the cross section), but any two atoms at sites i and j share this role, giving rise to a propagation of the photoelectron wave between them with a period given by $\Delta k = 2\pi/R_{ij}$. This case encompasses the emission from delocalized occupied states of diatomic molecules and characterizes the Cohen-Fano interference term as the lowest order of such new processes, rather than the realization of a microscopic Young's experiment.

We have clarified that the coherent emission from atomic sites does not necessarily require their equivalence. It is sufficient that the initial state be delocalized over different atomic sites, as shown clearly by the expression (12) and indicated by other authors [22].

In this context we have also elucidated the relation between intramolecular scattering from a single site and coherent interference originating from the new processes, accounting in this way for the experimental findings of Zimmermann and coworkers [6].

Finally, we have shown that the orientationally averaged scattering of electrons off small molecules (in particular diatomic molecules) can give access to CF oscillations, although in a more complicated way, due to the lack of site selectivity in comparison with the photoemission process and the absence of a dipole selection rule. This type of modulation has the same physical origin as that found in photoabsorption.

APPENDIX

1. Synopsis of multiple scattering theory

We summarize here, for the benefit of the reader, some of the aspects of MS theory useful for understanding its structure.

The method of MS transforms the Lippmann-Schwinger (LS) equation associated to the SE (2) in a set of algebraic equations for the amplitudes $B_L^i(\mathbf{k})$ which obey the MS equations

$$\sum_{L'} (T^i)^{-1}_{LL'} B_{L'}^i(\mathbf{k})$$

$$- \sum_{jL'} (1 - \delta_{ij}) G_{LL'}^{ij} B_{L'}^i(\mathbf{k}) = \sqrt{\frac{k}{\pi}} i^l Y_L(\hat{\mathbf{k}}) e^{i\mathbf{k}\cdot\mathbf{R}_i},$$

$$(\mathbf{T}^{-1} - \mathbf{G}) B(\mathbf{k}) = I(\mathbf{k}), \tag{A1}$$

in terms of the cell scattering matrix $T_{LL'}^i \delta_{ij}$ and the free spherical wave propagator (SWP) $G_{LL'}^{ij}$ coming from the free Green's Function of the LS equation. The term on the right-hand side stems from the impinging plane wave part of the continuum photoelectron state in Eq. (3). Due to the factor $(1 - \delta_{ij})$, one defines by convention $G_{LL'}^{ii} = 0$. The second equation writes the first in compact matricial form. We refer the interested reader to Ref. [35] for a derivation of the MS equations from the LS equation.

The cell scattering matrix $T_{LL'}^i$ in an angular momentum basis gives the scattering amplitude due to the (in general) anisotropic molecular potential in cell i of the photoelectron impinging on the cell with angular momentum L into a state of angular momentum L', whereas the free SWP $G_{LL'}^{ij}$ represents its amplitude of propagation from cell i, starting with angular momentum L, to cell j ending with angular momentum L'.

The solution for the amplitudes $B_L^i(\mathbf{k})$ is given by

$$B_L^i(\mathbf{k}) = \sqrt{\frac{k}{\pi}} \sum_{jL'} \tau_{LL'}^{ij} i^{l'} Y_{L'}(\hat{\mathbf{k}}) e^{i\mathbf{k}\cdot\mathbf{R}_j}, \tag{A2}$$

after introducing the scattering path operator $\boldsymbol{\tau}$, inverse of the MS matrix $(\mathbf{T}^{-1} - \mathbf{G})$

$$\boldsymbol{\tau} = (\mathbf{T}^{-1} - \mathbf{G})^{-1} = \sum_{n=0}^{\infty} (\mathbf{T}\mathbf{G})^n \mathbf{T} = \sum_{n=0}^{\infty} \mathbf{T} (\mathbf{G}\mathbf{T})^n, \tag{A3}$$

where the series expansion generates the Born series (matrix multiplication in the appropriate indexes is implied) and converges if $\rho(\mathbf{T}\mathbf{G})$, the spectral radius (maximum eigenvalue) of $\mathbf{T}\mathbf{G}$, is less than one.

It is clear that $\tau_{LL'}^{ij}$ obeys the following equation:

$$\tau_{LL'}^{ij} = T_{LL'}^i \delta_{ij} + \sum_{\underline{L}\underline{L}'k} T_{L\underline{L}}^i G_{\underline{L}\underline{L}'}^{ik} \tau_{\underline{L}'L'}^{kj}, \tag{A4}$$

which is derived from a resummation of the Born series in which the photoelectron first scatters from cell i, then propagates to cell k undergoing here another scattering event, then to the next cell, and so on and so forth.

The exact expression of the SWP, also known as real-space Korringa-Kohn-Rostoker (KKR) structure factors [36], is given by

$$G_{LL'}^{ij} = -4\pi i k \sum_{L''} i^{l-l'+l''} C_{LL'}^{L''} H_{L''}^+(\mathbf{R}_{ij}), \tag{A5}$$

where $H_L^+(\mathbf{R}) = h_l^+(kR) Y_L(\hat{\mathbf{R}})$, $h_l^+(kR)$ being the Hankel function of the first kind, and $\mathbf{R}_{ij} = \mathbf{R}_i - \mathbf{R}_j$ is the vector joining the origins of the cells Ω_i and Ω_j. Moreover, $C_{LL'}^{L''} = \int Y_L(\Omega) Y_{L'}(\Omega) Y_{L''}(\Omega) d\Omega$ is a Gaunt coefficient. We

use throughout real spherical harmonics (SH). A fairly good approximation to the SWP [9,37] is given by

$$G_{LL'}^{ij} \approx -4\pi\, k\, \frac{e^{ikR_{ij}}}{kR_{ij}}\, g_{ll'}^0(kR_{ij})\, Y_L(\hat{\mathbf{R}}_{ij})\, Y_{L'}(\hat{\mathbf{R}}_{ij})\, i^{(l-l')}. \quad \text{(A6)}$$

The function $g_{ll'}^0(\rho)$ represents a kind of curved wave correction [37] given by

$$g_{ll'}^0(\rho) = \left[1 + \frac{L^2 + (L')^2}{2\rho^2}\right]^{1/2} e^{i[L^2+(L')^2]/(2\rho)} J_0\left(\frac{L^2 L'^2}{\rho^2}\right), \quad \text{(A7)}$$

where J_0 is the spherical Bessel function of order zero and $L^2 = l(l+1)$.

The series expansion in Eq. (A3) is known as MS series, each terms being in one-to-one correspondence with the path followed by the photoemitted electron in its way out of the system. The various paths are ordered in amplitude in terms of the number of successive scattering undergone by the photoelectron, since each additional scattering costs in amplitude a factor $|TG| \approx \max|T_{LL}|/(kR)$ (the diagonal terms are always dominant).

Indeed, due to the anisotropy of the molecular potential, the scattering matrices $T_{LL'}$ are not diagonal in the angular momentum. The program calculates these cell matrices according to formulas (63), (64), and (71) of Ref. [12] in terms of the radial functions $R_{L'L}(r)$ of the local solutions of the Schrödinger equation $\Phi_L^n(\mathbf{r}) = \sum_{L'} R_{L'L}(r) Y_{L'}(\hat{r})$ $(n = 1, 2)$. At energies beyond roughly 100 eV the photoelectron barely sees the anisotropies of the potential, so that with increasing energy $T_{LL'} \approx t_l \delta_{LL'} = -1/k\, e^{i\delta_l} \sin \delta_l$ becomes almost diagonal and m independent. These t_l are the atomic scattering matrices of a spherically averaged muffin-tin potential, providing the associated phase shifts. The same behavior is seen in the eigenphase shifts obtained by diagonalizing directly the matrix $T_{LL'}$, which become almost m-independent with increasing energy.

In photoemission there are open and closed paths. A path is open when the last atom touched by the photoelectron before reaching the detector is different from the photoemitter, closed when the last atom coincides with the photoemitter. In photoabsorption, in the absence of an external detector, only closed paths are possible for emission from a single center, whereas in the case of multicenter emission other paths are possible that go from one emitter to the other, as illustrated in the body of the paper.

2. Exact expression of photoemission in homopolar diatomic molecules

The result in Eq. (18) would be exact if the photoemission amplitudes $\overline{B}_L(\mathbf{k})$ contained only closed multiple scattering paths [see Eqs. (A8) and (A9)]. However, the presence of paths connecting the two atomic sites destroys their equivalence with respect to periodicity.

In fact, with reference to Eq. (14), we have

$$\overline{B}_L^1(\mathbf{k}) = \sqrt{\frac{k}{\pi}} \sum_{L'} \left[\boldsymbol{\tau}_{LL'}^{11}\, i^{l'} Y_{L'}(\hat{\mathbf{k}}) + \boldsymbol{\tau}_{LL'}^{12}\, i^{l'} Y_{L'}(\hat{\mathbf{k}})\, e^{i\mathbf{k}\cdot\mathbf{R}}\right]. \quad \text{(A8)}$$

Similarly for $\overline{B}_L^2(\mathbf{k})$ we find

$$\overline{B}_L^2(\mathbf{k}) = \sqrt{\frac{k}{\pi}} \sum_{L'} \left[\boldsymbol{\tau}_{LL'}^{22}\, i^{l'} Y_{L'}(\hat{\mathbf{k}}) + \boldsymbol{\tau}_{LL'}^{21}\, i^{l'} Y_{L'}(\hat{\mathbf{k}})\, e^{-i\mathbf{k}\cdot\mathbf{R}}\right]. \quad \text{(A9)}$$

Notice the difference of the phase factor in the two expressions. To express the amplitude at site 2 in terms of that at site 1, we transform the last term of the second equation using the symmetry property of the scattering path operator in a real spherical harmonics basis: $\boldsymbol{\tau}_{LL'}^{21} = \boldsymbol{\tau}_{L'L}^{12} = (-1)^{l+l'} \boldsymbol{\tau}_{LL'}^{12}$, coming directly from the property of the spherical wave propagator $G_{LL'}^{ij}$. We find

$$\boldsymbol{\tau}_{LL'}^{21}\, i^{l'} Y_{L'}(\hat{\mathbf{k}}) = (-1)^l \boldsymbol{\tau}_{LL'}^{12}\, i^{l'} Y_{L'}(-\hat{\mathbf{k}}). \quad \text{(A10)}$$

As expected, the photoemission amplitude emanating from site 2 and going to site 1 is the same as that emanating from site 1 calculated at $-\mathbf{k}$, due to the presence of the inversion center midway the two atomic sites. The additional phase factor $(-1)^l$ takes into account the parity of the final state, selected by the dipole rule, with respect to the inversion symmetry.

As a consequence, putting $c_1 = c_2 = 1/\sqrt{2}$ in Eq. (17), defining for short $A_L^{ij}(\mathbf{k}) = \sqrt{\frac{k}{\pi}} \sum_{L'} \boldsymbol{\tau}_{LL'}^{ij}\, i^{l'} Y_{L'}(\hat{\mathbf{k}})$ and taking into account that $A_L^{11}(\mathbf{k}) = A_L^{22}(\mathbf{k})$ we find for the photoemission cross section

$$\frac{d\sigma}{d\hat{\mathbf{k}}} = 2\pi^2 \alpha\, \hbar\omega \left| \sum_L M_L^*(E) \left[(1 \pm e^{i\mathbf{k}\cdot\mathbf{R}}) A_L^{11}(\mathbf{k}) \right.\right.$$
$$\left.\left. + A_L^{12}(\mathbf{k})\, e^{i\mathbf{k}\cdot\mathbf{R}} \pm (-1)^l A_L^{12}(-\mathbf{k})\right]\right|^2. \quad \text{(A11)}$$

3. Integrated partial ionization cross sections

To get more insight into the confinement analysis of Ref. [17], we derive in our formalism the total integrated molecular cross section in terms of the integrated partial ionization cross sections $\sigma_l(\omega)$, where l is the angular momentum of the photolectronic wave referred to the molecular center. According to Dill [38] the total integrated unpolarized cross section is given by the expression

$$\sigma_{\text{tot}}(\omega) \propto \sum_{lmm_\gamma} \left|D_{lmm_\gamma}^{(-)\Gamma_0}\right|^2 = \sum_l \sigma_l(\omega), \quad \text{(A12)}$$

where the transition matrix element $D_{lmm_\gamma}^{(-)\Gamma_0} = \langle \Psi_{lm}^{(-)} | \mathbf{e} \cdot \mathbf{r} | \Psi_{\Gamma_0} \rangle$ is given in terms of the time reversal scattering states $\Psi_{lm}^{(-)}$ in response to a spherical wave $J_L(\mathbf{r}_o) = j_l(kr_o) Y_L(\mathbf{r}_o)$ referred to the molecular origin midway the two equivalent atoms and Ψ_{Γ_0} is the initial $1\sigma_g$ molecular state. Moreover, m_γ refers to the spherical component of the polarization vector $\mathbf{e}$. It is not hard to convince oneself [9] that the coefficients $B_L^i(\mathbf{k})$ in Eq. (A1) in Appendix A 1, which were calculated in response to a plane wave [Eq. (3)], when calculated in response to the

spherical component Λ of the plane wave become [39]

$$B_L^i(\Lambda) = \sqrt{\frac{k}{\pi}} \sum_{jL'} \boldsymbol{\tau}_{LL'}^{ij} J_{L'\Lambda}^{jo}, \tag{A13}$$

where $J_{L'\Lambda}^{jo}$ is the translation operator of Eq. (33). This is due to the relation [9]

$$\sum_{L'} J_{LL'}^{io} \, i^{l'} Y_{L'}(\hat{\mathbf{k}}) = i^l Y_L(\hat{\mathbf{k}}) \, e^{i\mathbf{k}\cdot\mathbf{R}_{io}}, \tag{A14}$$

and the fact that a plane wave is a linear combination of spherical waves $J_L(\mathbf{r}_o)$ with coefficients $i^l Y_L(\hat{\mathbf{k}})$.

Therefore, the integrated partial ionization cross section $\sigma_\lambda(\omega)$ (starting for simplicity from a σ_g initial state) is given by

$$\sigma_\lambda(\omega) \propto \sum_{m_\lambda m_\gamma} \left|M_{1m_\gamma}\right|^2 \left|B_{1m_\gamma}^1(\Lambda) + B_{1m_\gamma}^2(\Lambda)\right|^2. \tag{A15}$$

As a check, summing over λ and using the optical theorem of Eq. (10), which can also be written [39] as $\sum_\Lambda B_L^i(\Lambda) B_{L'}^j(\Lambda) = -\frac{1}{\pi} \Im \boldsymbol{\tau}_{LL'}^{ij}$ one recovers the total absorption cross section of Eq. (27)

$$\sigma_{\text{tot}}(\omega) \propto \sum_{m_\gamma} \left|M_{1m_\gamma}\right|^2 \left(\Im \boldsymbol{\tau}_{1m_\gamma\,1m_\gamma}^{11} + \Im \boldsymbol{\tau}_{1m_\gamma\,1m_\gamma}^{12}\right). \tag{A16}$$

To have an insight as to the origin of the Cooper-like minima of $\sigma_\lambda(\omega)$, we use in Eq. (A13) a renormalized Born approximation for $\boldsymbol{\tau}_{LL'}^{12}$, whereby $\boldsymbol{\tau}_{LL'}^{12} \approx t_l \sum_{L''} G_{LL''}^{12} \boldsymbol{\tau}_{L''L'}^{22}$. This form should be reasonably valid beyond ≈ 30 eV from the ionization edge, since it is first order only in the propagation G^{12} and of infinite order for all closed paths [34].

Indicating by $\mathbf{R}$ the vector joining the two atomic sites, we find

$$\sigma_\lambda(\omega) \propto P_f^2 \sum_{m_\gamma m_\lambda} |M_{1\,m_\gamma}|^2 \left|\sum_L \boldsymbol{\tau}_{1m_\gamma L}^{11} J_{L\,\Lambda}^{1\,o} + t_1 \frac{e^{ikR}}{kR} Y_{1m_\gamma}(\hat{\mathbf{R}}) \sum_{LL'} Y_L(\hat{\mathbf{R}}) \, i^{1-l} \boldsymbol{\tau}_{LL'}^{22} J_{L'\Lambda}^{2\,o}\right|^2$$

$$\propto P_f^2 \sum_{m_\gamma m_\lambda} \sigma_{m_\gamma}^{\text{at}}(\omega) \left||A_\lambda| \, e^{i\phi_\lambda} + \frac{e^{ikR}}{kR} \, |B_\lambda| \, e^{i\psi_\lambda}\right|^2$$

$$\propto P_f^2 \sum_{m_\gamma m_\lambda} \sigma_{m_\gamma}^{\text{at}}(\omega) \left[|A_\lambda|^2 + \frac{|B_\lambda|^2}{(kR)^2} + 2\,|A_\lambda||B_\lambda| \, \frac{\cos(kR + \eta_\lambda)}{kR}\right], \tag{A17}$$

where, for short, we have put $\eta_\lambda = \psi_\lambda - \phi_\lambda$,

$$A_\lambda = |A_\lambda| \, e^{i\phi_\lambda} = t_1^{-1} \sum_L \boldsymbol{\tau}_{1m_\gamma L}^{11} J_{L\,\Lambda}^{1\,o}, \tag{A18}$$

$$B_\lambda = |B_\lambda| \, e^{i\psi_\lambda} = Y_{1m_\gamma}(\hat{\mathbf{R}}) \sum_{LL'} Y_L(\hat{\mathbf{R}}) \, i^{1-l} \boldsymbol{\tau}_{LL'}^{22} J_{L'\Lambda}^{2\,o}, \tag{A19}$$

and we have dropped for simplicity the dependence of A_λ and B_λ on m_γ, m_λ.

The parity factor $P_f = 1 - (-1)^{\lambda-1}$ arises from the fact that Eq. (A15) provides four terms in the site indices 1 and 2 that are related by pairs by the factor $(-1)^{\lambda-1}$ due the symmetry properties of $\boldsymbol{\tau}$ and J. It is at this point that the global parity requirement for λ arises, as in Ref. [1].

[1] H. D. Cohen and U. Fano, Interference in the photo-ionization of molecules, Phys. Rev. **150**, 30 (1966).

[2] N. Stolterfoht, B. Sulik, V. Hoffmann, B. Skogvall, J. Y. Chesnel, J. Rangama, F. Frémont, D. Hennecart, A. Cassimi, X. Husson, A. L. Landers, J. A. Tanis, M. E. Galassi, and R. D. Rivarola, Evidence for interference effects in electron emission from H_2 colliding with 60 MeV/u Kr^{34+} ions, Phys. Rev. Lett. **87**, 023201 (2001).

[3] D. Rolles, Isotope-induced partial localization of core electrons in the homonuclear molecule N_2, Nature **437**, 711 (2005).

[4] D. Rolles, *Scattering and Coherence Phenomena in the Photoionization of Small Molecules*, Ph.D. thesis, Fritz Haber Institute (2005).

[5] M. F. Ciappina, O. A. Fojón, and R. D. Rivarola, Coherent electron emission from simple molecules by impact of energetic charged particles, J. Phys. B: At. Mol. Opt. Phys. **47**, 042001 (2014).

[6] B. Zimmermann, D. Rolles, B. Langer, R. Hentges, M. Braune, S. Cvejanovic, O. Geßner, F. Heiser, S. Korica, T. Lischke, A. Reinköster, J. Viefhaus, R. Dörner, V. McKoy, and U. Becker, Localization and loss of coherence in molecular double-slit experiments, Nat. Phys. **4**, 649 (2008).

[7] U. Becker, Matter-wave interference made clear, Nature **474**, 586 (2011).

[8] S. E. Canton, E. Plésiat, J. D. Bozek, B. S. Rude, P. Decleva, and F. Martin, Direct observation of Young's double-slit interferences in vibrationally resolved photoionization of diatomic molecules, Proc. Natl. Acad. Sci. USA **108**, 7302 (2011).

[9] D. Sebilleau, R. Gunnella, Z.-Y. Wu, S. Di Matteo, and C. R. Natoli, Multiple-scattering approach with complex potential in the interpretation of electron and photon spectroscopies, J. Phys.: Condens. Matter **18**, R175 (2006).

[10] A. Ankudinov, B. Ravel, J. J. Rehr, and S. D. Conradson, Real-space multiple-scattering calculations and interpretation

of x-ray absoprtion near-edge structure, Phys. Rev. B **58**, 7565 (1998).

[11] J. J. Rehr and R. C. Albers, Theoretical approaches to x-ray absorption fine structure, Rev. Mod. Phys. **72**, 621 (2000).

[12] K. Hatada, K. Hayakawa, M. Benfatto, and C. R. Natoli, Full-potential multiple scattering theory with space-filling cells for bound and continuum states, J. Phys.: Condens. Matter **22**, 185501 (2010).

[13] A. Filipponi, A. Di Cicco, and C. R. Natoli, X-ray-absorption spectroscopy and n-body distribution functions in condensed matter. I. Theory, Phys. Rev. B **52**, 15122 (1995).

[14] J. Xu, P. Krüger, C. R. Natoli, K. Hayakawa, Z. Wu, and K. Hatada, X-ray absorption spectra of graphene and graphene oxide by full-potential multiple scattering calculations with self-consistent charge density, Phys. Rev. B **92**, 125408 (2015).

[15] R. Broer and W. C. Nieuwpoort, Hole localization and symmetry breaking, J. Mol. Struct. (Theochem) **458**, 19 (1998).

[16] M. Ilchen, L. Glaser, F. Scholz, P. Walter, S. Deinert, A. Rothkirch, J. Seltmann, J. Viefhaus, P. Decleva, B. Langer, A. Knie, A. Ehresmann, O. M. Al-Dossary, M. Braune, G. Hartmann, A. Meissner, L. C. Tribedi, M. AlKhaldi, and U. Becker, Angular momentum sensitive two-center interference, Phys. Rev. Lett. **112**, 023001 (2014).

[17] J. Fernández, O. Fojón, A. Palacios, and F. Martín, Interferences from fast electron emission in molecular photoionization, Phys. Rev. Lett. **98**, 043005 (2007).

[18] L. Hedin and B. I. Lundqvist, Explicit local exchange-correlation potentials, J. Phys. C **4**, 2064 (1971).

[19] Y. Tikochinsky, Feynman rules for probability amplitudes, Int. J. Theor. Phys. **27**, 543 (1988).

[20] J. J. Barton, Photoelectron holography, Phys. Rev. Lett. **61**, 1356 (1988).

[21] C. S. Fadley, S. Thevuthasan, A. P. Kaduwela, C. Westphal, Y. J. Kim, R. Ynzunza, P. Len, E. Tober, F. Zhang, Z. Wang, S. Ruebush, A. Budge, and M. A. Van Hove, Photoelectron diffraction and holography: Present status and future prospects, J. Electron Spectrosc. Relat. Phenom. **68**, 19 (1994).

[22] P. Krüger, Photoelectron diffraction from valence states of oriented molecules, J. Phys. Soc. Jpn. **87**, 061007 (2018).

[23] A. S. Baltenkov, U. Becker, S. T. Manson, and A. Z. Msezane, Interference in the molecular photoionization and Young's double-slit experiment, J. Phys. B: At. Mol. Opt. Phys. **45**, 035202 (2012).

[24] R. Della Picca, P. D. Fainstein, M. L. Martiarena, N. Sisourat, and A. Dubois, Cooper minima and Young-type interferences in photoionization of one-electron molecular ions, Phys. Rev. A **79**, 032702 (2009).

[25] D. P. Woodruff, Analysis of photoelectron diffraction spectra using single scattering simulations, Surf. Sci. **166**, 377 (1986).

[26] X.-J. Liu, N. A. Cherepkov, S. K. Semenov, V. Kimberg, F. Gelmukhanov, G. Prümper, T. Lischke, T. Tanaka, M. Hoshino, H. Tanaka, and K. Ueda, Young's double-slit experiment using core-level photoemission from N_2: Revisiting Cohen-Fano's two-centre interference phenomenon, J. Phys. B: At. Mol. Opt. Phys. **39**, 4801 (2006).

[27] J. L. Dehmer and Dan Dill, Molecular effects on inner-shell photoabsorption: K shell spectrum of N_2, J. Chem. Phys. **65**, 5327 (1976).

[28] N. A. Cherepkov, S. K. Semenov, Y. Hikosaka, K. Ito, S. Motoki, and A. Yagishita, Manifestation of many-electron correlations in photoionization of the K shell of N_2, Phys. Rev. Lett. **84**, 250 (2000).

[29] S. K. Semenov, N. A. Cherepkov, M. Matsumoto, T. Hatamoto, X.-J. Liu, G. Prümper, T. Tanaka, M. Hoashino, H. Tanaka, F. G. Mukhanov, and K. Ueda, Interference modulation in the vibrationally resolved photoionization of the σ_g and σ_u levels of the N_2 molecule, J. Phys. B: At. Mol. Opt. Phys. **39**, L261 (2006).

[30] S. T. Pratt, Excited-state molecular photoionization dynamics, Rep. Prog. Phys. **58**, 821 (1995).

[31] D. Dill and J. L. Dehmer, Electron-molecule scattering and molecular photoionization using the multiple-scattering method, J. Chem. Phys. **61**, 692 (1974).

[32] C. R. Natoli, M. Benfatto, C. Brouder, M. F. RuizLópez, and D. L. Foulis, Multichannel multiple-scattering theory with general potentials, Phys. Rev. B **42**, 1944 (1990).

[33] W. J. Moore, *Physical Chemistry*, 2nd ed. (Prentice-Hall, Englewood Cliffs, NJ, 1955), pp. 848–856.

[34] A. Messiah, *Quantum Mechanics*, (North-Holland, Amsterdam, 1970), Vol. II, pp. 848–856.

[35] D. Sébilleau, K. Hatada, and H. Ebert, *Multiple Scattering Theory for Spectroscopies: A Guide to Multiple Scattering Computer Codes*, of *Springer Proceedings in Physics* (Springer International Publishing, Cham, 2018) Vol. 204.

[36] W. Kohn and N. Rostoker, Solution of the Schrödinger equation in periodic lattices with an application to metallic lithium, Phys. Rev. **94**, 1111 (1954).

[37] J. J. Rehr, R. C. Albers, C. R. Natoli, and E. A. Stern, New high-energy approximation for x-ray-absorption near-edge structure, Phys. Rev. B **34**, 4350 (1986).

[38] D. Dill, Fixed-molecule photoelectron angular distributions, J. Chem. Phys. **65**, 1130 (1976).

[39] C. R. Natoli, M. Benfatto, and S. Doniach, Use of general potentials in multiple-scattering theory, Phys. Rev. A **34**, 4682 (1986).